Journal of Orthopaedic Translation 49 (2024) 264–282

Contents lists available at ScienceDirect

Journal of Orthopaedic Translation

journal homepage: www.journals.elsevier.com/journal-of-orthopaedic-translation

Original Article

Mesoporous bioactive glass-enhanced MSC-derived exosomes promote bone regeneration and immunomodulation in vitro and in vivo

Qingde Wa [a,b,1], Yongxiang Luo [c,1], Yubo Tang [d,1], Jiaxiang Song [a], Penghui Zhang [e], Xitao Linghu [a], Sien Lin [f,g], Gang Li [f,g], Yixiao Wang [h], Zhenyu Wen [i], Shuai Huang [j,2,**], Weikang Xu [b,k,l,2,*]

[a] Department of Orthopaedic Surgery, The Second Affiliated Hospital of Zunyi Medical University, Zunyi, Guizhou, China. Intersection of Xinlong Avenue and Xinpu Avenue, Honghuagang District, Zunyi, Guizhou, 563000, China
[b] Institute of Biological and Medical Engineering, Guangdong Academy of Sciences, No.10 Shiliugang Road, Jianghai Avenue Central, Haizhu District, Guangzhou, Guangdong, 510316, China
[c] Marshall Biomedical Engineering Laboratory, Shenzhen University, No. 3688 Nanhai Avenue, Nanshan District, Shenzhen, Guangdong, 518060, China
[d] Department of Pharmacy, The First Affiliated Hospital of Sun Yat-sen University, No.58 Zhongshan Second Road, Guangzhou, Guangdong, 510080, China
[e] Department of Orthopaedics, Seventh Affiliated Hospital of Sun Yat-sen University, No. 628, Zhenyuan Road, Xinhu Street, Guangming District, Shenzhen, Guangdong, 518107, China
[f] Musculoskeletal Research Laboratory, Department of Orthopaedics and Traumatology, The Chinese University of Hong Kong, Prince of Wales Hospital, Hong Kong, China
[g] Stem Cells and Regenerative Medicine Laboratory, Li Ka Shing Institute of Health Sciences, The Chinese University of Hong Kong, Prince of Wales Hospital, Hong Kong, China
[h] Department of Orthopaedic Surgery, The Third Affiliated Hospital of Zunyi Medical University, Zunyi, Guizhou, China, No. 98 Fenghuang North Road, Huichuan District, Zunyi City, Guizhou, 563002, China
[i] Zunyi Medical University, No. 1 Campus, Xinpu New District, Zunyi City, Guizhou, 563000, China
[j] Department of Orthopaedic Surgery, The Second Affiliated Hospital of Guangzhou Medical University, No. 250 Changgang East Road, Haizhu District, Guangzhou, Guangdong, 510260, China
[k] National Engineering Research Center for Healthcare Devices, Guangdong Key Lab of Medical Electronic Instruments and Polymer Material Products, Guangdong Institute of Medical Instruments, No. 1307 Guangzhou Avenue Central, Tianhe District, Guangzhou, Guangdong, 510500, China
[l] Guangdong Chinese Medicine Intelligent Diagnosis and Treatment Engineering Technology Research Center, No. 10 Shiliugang Road, Jianghai Avenue Central, Haizhu District, Guangzhou, Guangdong, 510316, China

ARTICLE INFO

Keywords:
Ex vivo bone regeneration
Mesoporous bioactive glass
MSC-Derived exosomes
Immunomodulation
Vascular regeneration

ABSTRACT

Background: Exosomes produced by mesenchymal stem cells (MSCs) have vascular generative properties and are considered new effective candidates for the treatment of bone defects as alternatives to cell therapy. Improving the pro-regenerative function and efficacy of exosomes has been a popular research topic in the field of orthopaedics.

Methods: We prepared mesoporous bioactive glass (mBG) microspheres via the template method. The ionic products of mBGs used to treat MSCs were extracted, and the effects of exosomes secreted by MSCs on osteoblast (OB) and macrophage (MP) behaviour and bone defect repair were observed in vivo (Micro-CT, H&E, Masson, and immunofluorescence staining for BMP2, COL1, VEGF, CD31, CD163, and iNOS).

Results: The mBG spheres were successfully prepared, and the Exo-mBG were isolated and extracted. Compared with those in the blank and Exo-Con groups, the proliferation and osteogenic differentiation of OBs in the Exo-mBG group were significantly greater. For example, on Day 7, OPN gene expression in the Ctrl-Exo group was 3.97 and 2.83 times greater than that in the blank and Exo-mBG groups, respectively. In a cranial defect rat model, Exo-mBG promoted bone tissue healing and angiogenesis, increased M2 macrophage polarisation and

* Corresponding author. Institute of biological and Medical Engineering, Guangdong Academy of Sciences, Jianghai Avenue Central, Haizhu District, Guangzhou, Guangdong, 510316, China.
** Corresponding author. Department of Orthopaedic Surgery, the Second Affiliated Hospital of Guangzhou Medical University, No. 250 Changgang East Road, Haizhu District, Guangzhou, Guangdong, 510260, China.
E-mail addresses: huang-shuai@hotmail.com (S. Huang), 759200816@qq.com, weikangxu1987@hotmail.com (W. Xu).
[1] These authors contributed equally to this work.
[2] Present address: Jianghai Avenue Central, Haizhu District, Guangzhou, Guangdong 510316, China.

https://doi.org/10.1016/j.jot.2024.09.009
Received 2 June 2024; Received in revised form 8 September 2024; Accepted 23 September 2024
Available online 29 October 2024

inhibited M1 macrophage polarisation, as verified by micro-CT, H&E staining, Masson staining and immunofluorescence staining. These effects may be due to the combination of a higher silicon concentration and a higher calcium-to-phosphorus ratio in the mBG ionic products.
Conclusion: This study provides insights for the application of exosomes in cell-free therapy and a new scientific basis and technical approach for the utilisation of MSC-derived exosomes in bone defect repair.
The translational potential of this article: Our study demonstrated that exosomes produced by mBG-stimulated MSCs have excellent in vitro and in vivo bone-enabling and immunomodulatory functions and provides insights into the use of exosomes in clinical cell-free therapies.

1. Introduction

The treatment of large bone defects caused by severe fracture trauma, postoperative bone tumours or the removal of osteomyelitis lesions and congenital bone tissue defects has always been a major challenge in orthopaedic clinics [1]. Bone nonunion and large bone defects, especially in load-bearing areas, can seriously affect the health of patients and reduce their quality of life. Autologous and allogeneic bone grafting, as the gold standard in the treatment of bone defects, can often achieve satisfactory treatment results [2]. However, autologous bone grafts often cause complications such as pain and discomfort in the bone harvesting area, limited bone harvesting, bone fracture at the harvesting site, haematomas and infections [3]. Moreover, allogeneic bone grafts have disadvantages such as a high likelihood of rejection, slow healing of bone defects, and increased costs [4]. Stem cell transplantation therapy exploits the multidirectional differentiation potential and self-replicating ability of stem cells to repair tissue damage and is an advanced medical technology that is currently effective at promoting fracture healing [5]. Mesenchymal stem cells (MSCs) are pluripotent stem cells with multilineage differentiation and immunomodulatory capabilities that are widely present in various tissues and have the potential to promote tissue regeneration [6]. However, research reports have shown that stem cell transplantation still faces some obstacles in specific technical applications, such as a low survival rate of transplanted cells, innate heterogeneity, unknown factors related to the age of the donor, and potential carcinogenicity [7].

MSCs act mainly in a paracrine manner, and their secreted mediators are important facilitators of tissue repair and wound healing [8]. Exosomes are subcellular double-layer membrane extracellular vesicles (EVs) with molecular diameters of 40–200 nm that are formed and secreted by cells through the process of endocytosis–fusion–exocytosis. Exosomes mainly contain cytokines and growth factors similar to those of the cells from which they originate, and the microenvironment in which they are embedded regulates the growth and function of effector cells [9]. Numerous studies have demonstrated that exosomes derived from MSCs are involved in a wide range of biological processes by influencing tissue responses to injury, infection and disease and that while exosomes possess the therapeutic properties of stem cells, they do not exert the same detrimental effects as direct stem cell implantation [9,10]. As major paracrine effectors of cells, exosomes have received increasing attention for their ability to promote fracture healing [11]. Studies have shown that exosomes applied in bone tissue repair can promote cell proliferation and migration during bone formation, as well as osteogenesis and angiogenesis [12]. Although the value of exosomes for clinical tissue repair applications has long been noted, their use in practice is still severely limited by the difficulty of producing large amounts of exosomes [13,14]. This limitation is mainly due to 1) the inefficiency of current methods for extracting and purifying exosomes and 2) the weak ability of cells to produce exosomes themselves [15,16]. Moreover, understanding how to enhance the specific functions of exosomes to improve their ability to repair tissue defects in different fields is a current research hotspot. Therefore, improving the ability of cells to produce exosomes and enhancing the biological functions of exosomes by modifying cells or adjusting the cellular microenvironment are key strategies for obtaining sufficient exosomes with enhanced functions for regenerative medicine.

The secretion of exosomes is related to a variety of factors, including cell type, cell state, and the microenvironment in which the cell is located. When the microenvironment of a cell changes, its ability to secrete exosomes and the biological function of the secreted exosomes change substantially. For example, in a low-oxygen microenvironment, the ability of amniotic fluid stem cells, human bone marrow mesenchymal stem cells, human monocytes, rat myocardial precursor cells, and rat cardiomyocytes to secrete exosomes is significantly increased, and their secreted exosomes significantly enhance myocardial repair, vascularisation, and wound healing [17,18]. When the active signals of biomaterials are released into the microenvironment, they can, on the one hand, directly act on the cells and affect their growth; on the other hand, the biomaterials can change the microenvironment in which the cells are located, thus indirectly affecting cell growth. Additionally, exosome release and phenotype may be affected after the administration of biomaterials. For example, Ruan et al. reported that a traditional Chinese medicine, a quick-acting heart-saving pill used to treat acute myocardial ischaemia, significantly increased exosome secretion in mouse cardiac myocytes [19]. Shyong et al. reported that the release of calcium-containing microparticles into the cytoplasmic environment after the phagocytosis of calcium phosphate microparticles increased the secretion of exosomes by more than 2-fold; moreover, there was no significant difference in the level of calcium in the secreted exosomes under pathological or conventional conditions [20]. Bioactive glass (BG) has been clinically applied as a bone and dental defect repair material for many years because of its excellent osteogenic activity and osteoinductivity and has also been a hot research topic in recent years [21]. After decades of development, research on BG has progressed through three generations, namely, the first generation of 45S5-fused BG, the second generation of sol–gel (SBG), and the third generation of mesoporous bioactive glass (mBG) prepared via the sol–gel method in combination with the template method. With the recent iterations of the preparation process, the energy consumption for preparing BGs has decreased, and the surface area, dispersion, ion diffusion rate, biomineralisation rate, and bioactivity of BG materials have significantly improved [22]. Ions produced by BG can activate multiple osteogenesis-related signalling pathways, thereby promoting the entry of relevant transcription factors into the nucleus to bind to promoters or enhancers of downstream genes, resulting in the upregulation of osteogenesis-related genes and increased protein synthesis to facilitate the mineralisation of cells for osteogenesis [23]. Zhi Wu et al. reported that the 45S5-fused BG ion product significantly improved exosome production by MSCs and further enhanced the ability of exosomes to promote vascularisation and angiogenesis in cortical bone by modifying exosome function [24]. However, there are still very few reports on the effects of biomaterials on cellular exosome secretion and even fewer reports on which mBG ionic products improve the osteoinductive regenerative effects of exosomes from MSCs in vitro and in vivo.

The excessive immune–inflammatory response that occurs during bone defect regeneration is another treatment challenge. While inflammation is a mechanism for the early initiation of healing, timely and effective resolution of inflammation is necessary for the formation of a pro-bone regenerative environment [25]. Macrophages (MPs) play an important role in the process of immune regulation, mainly via

polarisation to the M1 and M2 phenotypes. M1 macrophages are proinflammatory cells that recruit inflammatory factors to activate the immune response early during inflammation and resist pathogen invasion, but excessive inflammation causes tissue fibrosis and delayed healing. In contrast, M2 macrophages are cells with powerful anti-inflammatory effects and are involved mainly in the clearance of inflammatory factors, tissue healing and remodelling, and immunomodulation [26]. Therefore, biomedical materials must be able to modulate M1-to-M2 macrophage polarisation. Similarly, the environment surrounding bone defects can affect bone repair. In pathological bone defects, such as defects associated with osteoporosis and tumours, osteoclasts are abnormally active and adhere to bone tissue to promote bone resorption and affect bone regeneration [27].

In summary, we hypothesised that cellular exosome production and the osteogenic activity of exosomes could be simultaneously enhanced by mBG. mBG ion products were used to stimulate MSCs. Exosomes produced by MSCs stimulated with or without mBG ion products were analysed, and the ability of these exosomes to promote osteoblast (OB) differentiation was assessed. The results showed that mBG ion products significantly promoted exosome production by MSCs. In addition, compared with conventional exosomes from MSCs, exosomes from MSCs stimulated with mBG ionic products had an improved ability to promote osteogenic differentiation in vitro and bone and vascular regeneration in vivo. Surprisingly, these exosomes promoted M2 polarisation and inhibited M1 polarisation in macrophages. These results support our hypothesis that mBG ion products significantly increase the production of exosomes while improving their biological functions. Our findings also suggest that cell stimulation with mBG is a safe and viable method for modulating exosome secretion and enhancing its practical application in the field of bone repair.

2. Materials and methods

2.1. Materials

Dodecylamine (DDA) and triethyl phosphate (TEP) were purchased from Aladdin Bio-Chem Technology Co., Ltd. Ethyl orthosilicate (TEOS), calcium nitrate tetrahydrate (CN), and anhydrous ethanol were purchased from Guangzhou Chemical Reagent Factory. High-glucose Dulbecco's modified Eagle's medium (DMEM; Gibco), phosphate-buffered saline (PBS; Gibco), foetal bovine serum (FBS; 10270-106; Gibco), RIPA lysis buffer (Beyotime), a cell counting kit-8 (CCK-8; Dojindo Laboratories), an alkaline phosphatase (ALP) test kit (Beyotime), a total protein quantification kit (Thermo Fisher) and Alizarin red S (ARS; Sigma Aldrich) were used. Rat MSCs and OBs were purchased from American Type Culture Co. (ATCC, Manassas, VA). Mouse RAW 267.4 (MPs) was purchased from Tongpai Biotechnology Co. (Shanghai, China).

2.2. Cell culture

MSCs, MPs and OBs were cultured in DMEM supplemented with 10 % FBS and 1 % penicillin/streptomycin. All of the cells were kept at 37 °C in an incubator with 5 % CO_2 and high humidity. The culture medium was replaced every two days. Cell subculturing was performed after the cells reached 75–85 % confluence. For all the experiments in this study, only early-passage MSCs and OBs (passages 2–5) were used. Referring to the literature, we performed ALP staining and calcium nodule staining on OBs on Days 3 and 7, respectively, to determine that within this timeframe, OBs are able to undergo osteogenic differentiation and produce calcium nodules under normal culture conditions [28].

2.3. Preparation and characterisation of mBG and its ionic products

2.3.1. Preparation of mBG and its ionic products

The molar percentage of the chemical composition of the mBG was SiO_2:CaO:P_2O_5 = 80:15:5. The specific preparation procedure was as follows: first, 40 g of DDA was dissolved in 250 ml of deionised water and 800 ml of anhydrous ethanol. After stirring for 10 min, TEOS (160 ml), TEP (104.9 ml) and CN (242.1 g) were added sequentially to the solution, and each reagent was stirred for 30 min before the next agent was added slowly. Stirring was continued for 3 h, after which the mixture was incubated for 24 h. The resulting precursors were centrifuged and washed three times alternately with deionised water and anhydrous ethanol. Finally, the powder precursor was put into a muffle furnace and heated at 650 °C for 3 h to obtain the mBG powder.

One hundred milligrams of mBG powder was added to 10 mL of basal DMEM and incubated in a humidified 37 °C/5 % CO_2 incubator for 24 h. Then, the supernatant was collected, centrifuged at 1000×*g* for 10 min and sterilised through a filter (Millipore, 0.22 μm). The ionic product of mBG was obtained.

2.3.2. Characterisation of mBG and its ionic products

The microscopic morphology of the mBG microspheres was observed and characterised via a high-resolution field emission scanning electron microscope (Merlin) from Carl Zeiss, Germany. The samples were plated with platinum to ensure suitable electrical conductivity. The mBG microspheres were characterised via transmission electron microscopy (JEM-2100HR) from JEOL Ltd. Additionally, the mBG microspheres were characterised via a nanosize zeta potential tester (Zetasizer NanoZS) from Malvern Instruments. The mBG mesopore structure was characterised by a NOVA4200e analyser, a specific surface area and pore size analyser from Kantar Instruments, USA. The test conditions were 250 °C for 4 h. The N_2 adsorption−desorption curves of the materials were analysed to calculate the specific surface area, average pore size and distribution of the materials. mBG was characterised by an X-ray diffractometer (Empyrean Sharpshooter) from Panacor, Netherlands, with a continuous scanning range from 1° to 10° and 10° to 80°, respectively, and a scanning speed of 2°/min. The mesoporous and phase structures of the materials were analysed via X-ray diffraction (XRD). mBG was characterised by a Fourier transform infrared spectrometer (CCR-1) from Thermo-Nicolet, USA, and the chemical bonding present in the samples was determined by analysing the characteristic peaks of the infrared absorption spectra. The concentrations of Ca, Si and P were determined via inductively coupled plasma−optical emission spectroscopy (ICP−OES; Agilent 5110, USA).

The mBG ion products were diluted 4-fold for further use, and the concentrations of the different ion types in the BG ion products are

Table 1
Sequences of the primers used for real-time polymerase chain reaction (PCR).

Genes	Primer sequences
Glyceraldehyde-3-phosphate dehydrogenase (GAPDH)	Forward: 5'-TGACCACAGTCCATGCCATC-3' Reverse: 5'-GACGGACACATTGGGGGTAG-3'
Alkaline phosphatase (ALP)	Forward: 5'-TTCATAATTCCAGGCCGAAC-3' Reverse: 5'-GGACGCTGACGAAGTACCAT-3'
Runt-related transcription factor 2 (RUNX2)	Forward: 5'-ATACTCTCCTGGGACTGTTTTCG-3' Reverse: 5'-GATGTTGCTCTGTTCGTIITCTT-3'
Bone morphogenetic protein 2 (BMP2)	Forward: 5'-TGAACACAGCTGGTCTCAGG-3' Reverse: 5'-ACCCCACATCACTGAAGTCC-3'
Collagen Type I COLI	Forward: 5'-TTCTCCTGGCAAAGACGGAC-3' Reverse: 5'-CTCAAGGTCACGGTCACGAA-3'
Osteopontin (OPN)	Forward: 5'-TGCAAACACCGTTGTAACCAAAAGC-3' Reverse: 5'-TGCAGTGGCCGTTTGCATTTCT-3'
CD206	Forward: ATGGATGTTGATGGCTACTGG Reverse: TTCTGACTCTGGACACTTGC
Arginase (ARG)	Forward: CATATCTGCCAAAGACATCG Reverse: CATATCTGCCAAAGACATCG
Tumour necrosis factor-α (TNF-α)	Forward: GGGTGTTCATCCATTCTC Reverse: GGTCACTGTCCCAGCAT
Interleukin-1 beta (IL-1β)	Forward: TACAGGCTCCGAGATGAACA Reverse: AGGCCACAGGTATTTTGTCG

shown in Table 2. The mBG extract was diluted and supplemented with FBS to a concentration of 10 % and used to culture MSCs and assay the proliferative properties and ALP activity of the cells. MSCs not treated with mBG ionic products were labelled the Ctrl group, and MSCs treated with mBG ionic products were labelled the mBG group. The proliferation of MSCs was measured at 1, 3, and 7 days via a Cell Counting Kit 8 (CCK-8) assay. At the designated times, the cells were washed twice with PBS, and CCK-8 assay solution (10 % (v/v)) in growth medium was added to each plate and incubated for 2 h. The proteins were subsequently transferred to a 96-well flat-bottomed plate, after which the absorbance was measured at a wavelength of 450 nm. A cell viability assay of MSCs was performed by staining the cells with AMPI. Subsequently, the morphology and distribution of the cells were observed with an inverted fluorescence microscope. Selected cells were tested after 72 h of adhesion and proliferation. ALP activity was used to determine the osteogenic differentiation capacity of the cells after 7 and 14 days of in vitro culture. Alizarin red S (0.5 %, pH 4.2; Sigma–Aldrich) was used to assess matrix mineralisation after 14 days. ALP activity was used to determine the osteogenic differentiation capacity of the cells in vitro. Specifically, the cells were washed three times with ice-cold PBS after 7 days of culture, and the plates were placed on ice. To each well, 400 μL of lysate containing 1 % PMSF was added, and the cells were lysed on ice for 30 min. The cells were subsequently centrifuged at 14 000 rpm for 10 min, and the supernatant was aspirated to obtain the total proteins, which were placed in the refrigerator at −80 °C for later use. The total protein concentration was determined with a BCA kit following the manufacturer's instructions, ALP was quantified with a Biyuntian ALP kit following the manufacturer's instructions, and ALP activity was calculated as the ratio of the ALP concentration to the total protein concentration. At predetermined time points (Days 7 and 14), qRT−PCR was used to measure the expression of the typical osteogenesis-related genes bone morphogenetic protein 2 (BMP2), alkaline phosphatase (ALP), osteopontin (OPN), collagen type I (COL1), and runt-related transcription factor 2 (RUNX2).

2.4. Exosome isolation

Complete medium with and without mBG ionic products was used to culture the MSCs. The isolation and characterisation of exosomes in this study followed the latest guidelines from the International Society for Extracellular Vesicles (MISEV2018, PMID 30637094). MSCs were stimulated with mBG ion products for 7 days, and the exosomes released by MSCs in the supernatant were isolated via a method combining conventional ultracentrifugation and ultrafiltration. MSCs were seeded at a density of 5×10^3 cells per square centimetre and cultured in total DMEM for 24 h. Then, the medium was removed, and the cells were washed three times with PBS (Invitrogen) before fresh basal DMEM with or without mBG ion products was added. After another 7 days of culture, the medium was changed to serum-free medium, and the cells were cultured for another 24 h. Subsequently, the culture supernatant was collected. Then, the collected culture supernatant was first centrifuged at 300×*g* for 10 min, 2000×*g* for 20 min and 10 000×*g* for 30 min at 4 °C and filtered through a 0.22 μm Steritop™ filter (Millipore) to remove cells, dead cells, cell debris and large vesicles, respectively. The supernatant was then ultracentrifuged at 100000×*g* for 2 h at 4 °C to remove soluble components such as proteins and to pellet the exosomes. Afterwards, the exosome pellets were resuspended in PBS. Finally, the exosome pellets were concentrated with an ultrafiltration device until the volume of the solution in the upper compartment was reduced to approximately 200 μL. The obtained mBG-stimulated MSC-derived exosomes were named Exo-mBG, and the conventionally cultured MSC-derived exosomes were named Exo-Con; these exosomes were stored at −80 °C or used for characterisation or further study.

Table 2
The concentrations of different types of ions in the mBG ion products.

Sample	Ca (ppm)	P (ppm)	Si (ppm)
Basal DMEM	75.66	28.75	0.16
1/4 mBG in basal DMEM	70.31	22.88	17.59

2.5. Exosome loading and release

For the animal experiments, injectable and in situ light-cured methacrylated silk (SilMA) was used as the carrier material for the exosomes. Specifically, a 0.25 % aqueous PBS solution of the photoinitiator lithium phenyl-2,4,6-trimethylbenzoylphosphinate (LAP) was prepared. At room temperature, SilMA was dissolved in LAP solution, and exosome-containing PBS was added so that the concentration of exosomes in the final solution was 2 mg/ml and the concentration of SilMA was 10 %.

The in vitro release profile of exosomes from SilMA was evaluated. Briefly, the hydrogels were placed in test tubes and immersed in 2 mL of PBS at 37 °C under constant vibration at 30 rpm. At each time point, all the supernatant was collected and replaced with an equal amount of fresh PBS. The number of released exosomes was quantified via nanoparticle tracking analysis (NTA; NanoSight NS300, Malvern, UK) to plot the release profile.

2.6. Characterisation of exosomes

2.6.1. Morphological observation

Transmission electron microscopy (TEM) was used to observe the morphology of the MSC-derived exosomes via transmission electron microscopy (Nikon Electronics Corporation JEM-1200EX). Briefly, the isolated exosome pellets were first negatively stained with 3 % phosphotungstic acid for 30 s and applied to a continuous carbon grid, followed by visualisation via transmission electron microscopy (TEM), after which images were taken.

2.6.2. Size distribution and purity detection

The collected exosome suspension was diluted 10-fold, and 50 μL of the diluted sample was subjected to high-sensitivity flow cytometry (HSFCM) for size analysis and particle concentration measurement [11]. For purity detection, another 50 μL of the diluted sample solution was incubated with 50 μL of 2.0 % (vol/vol) Triton X-100 at 37 °C for 1 h, followed by three washes with PBS to remove Triton X-100 and the addition of 50 μL Amicon Ultra-15 Centrifugal Units. The particle concentration was subsequently measured via HSFCM, and the purity of the isolated exosomes was calculated as the percentage of vesicles (%) [29].

2.7. In vitro study of exosomal osteogenic and immunomodulatory properties

MSC-derived exosomes were cocultured with OBs, and then mBG ion products were administered to investigate their effects on exosome osteogenic function. First, the blank (no exosome group), Exo-Con (exosomes derived from MSCs were added) and Exo-mBG (exosomes produced from MSCs stimulated with the addition of mBG ionic products) groups were used for the cell experiments.

The proliferation of OBs was measured at 1, 3, and 7 days via a CCK-8 assay.

OBs were plated in 48-well plates at a seeding density of 5×10^4 cells per well. After 24 h of adhesion, the medium was replaced with DMEM with or without exosomes. At predetermined time points, qRT−PCR was used to measure the expression of the typical osteogenesis-related genes BMP2, ALP, OPN, COL1, and RUNX2.

RAW264.7 cells were inoculated in 24-well plates at a density of 5×10^4 cells per well. After 24 h of adhesion, the medium was replaced with DMEM with or without exosomes, and the mixture was cultured for a total of 1 or 3 days. IL-10 and IL-12 expression in RAW264.7 cells was determined via enzyme-linked immunosorbent assay (ELISA) with IL-10

and IL-12 kits. The operation of the quantified IL-10 kit was performed according to the manufacturer's instructions. Real-time fluorescence quantitative PCR was used to detect the M1 immunomarker genes Tumour necrosis factor-alpha (TNF-α) and Recombinant Human Interleukin-1 beta (IL-1β); the M2 immunomarker genes CD206 and arginase (Arg) and glyceraldehyde phosphate dehydrogenase (GAPDH) were used as internal reference genes.

Briefly, total RNA was isolated via an RNA isolation kit (CW0581M) according to the manufacturer's protocol. After RNA isolation, DNase I treatment was performed, and the total RNA concentration and purity were measured at 260 nm via a Nanodrop spectrophotometer (Thermo). For the reverse transcription (RT) reaction, cDNA was synthesised from 1 mg of total RNA via the HIFI cDNA synthesis kit (CW2569M). Quantitative reverse transcriptase–polymerase chain reaction (qRT–PCR) amplification was performed with an Applied Biosystems QuantStudio 6 Flex Real-Time PCR (Thermo) using UltraSYBR Mixture (Low ROX) (CW2601M). The sequences of the forward and reverse primers used are listed in Table 1. Relative mRNA levels were calculated and normalised to those of GAPDH. Six qRT–PCR assays were performed.

RAW264.7 cells were inoculated into 48-well plates at a density of 5 $\times$ 10^4 cells per well, and complete medium was added and incubated for 1 day. The medium was subsequently aspirated and washed with PBS, followed by the addition of 50 μl of trypsin to each well and then 50 μl of complete medium to terminate the digestion, followed by the addition of 900 μl of 4 °C PBS to each well. The cells were detached by gentle blowing and centrifuged at 300×*g* for 5 min. The cells were resuspended in 1 % BSA/PBS, and 0.25 μg of the corresponding CD11c antibody (M1 marker, Invitrogen) and CD206 antibody (M1 marker, Invitrogen) were added to each well. Each well was incubated with 0.25 μg of the corresponding CD11c antibody (M1 marker; Invitrogen) or CD206 antibody (M2 marker; Invitrogen) for 30 min on ice in the dark. After incubation, the cells were centrifuged at 500×*g* for 2 min, and the supernatant was aspirated, resuspended in PBS, and then detected via a flow cytometer (BD FACSCelesta, BD, USA).

ALP activity was used to determine the osteogenic differentiation capacity of the cells after 3 and 7 days of in vitro culture. Alizarin red S was used to assess matrix mineralisation after 7 days.

Moreover, the cytotoxicity and cytocompatibility of the four groups were investigated via animal experiments. For the cytotoxicity experiments, the test samples, negative controls (high-density polyethylene), and positive controls (phenol) were immersed in DMEM containing 10 % foetal bovine serum at 37 °C for 24 h. During the maceration process, the concentrations of the test samples, negative controls and positive controls in the medium were 0.2 g/mL, 0.3 g/mL and 3 g/L, respectively. After the monolayer of OBs was raised, the original culture mixture was aspirated; the sample immersion solution, negative control, positive control, and blank control were added; and the samples were incubated at 37 °C for 24 h in a 5 % CO_2 incubator with a CCK-8 kit for detection. The formula of the relative growth rate (RGR) is as follows: RGR (%) = (OD value of the experimental group/OD value of the negative control group) × 100. The cytotoxicity of the samples was evaluated according to the standards of the American Pharmacopoeia [30]. Briefly, (i) RGR≥75 %, cytotoxicity grade 0 or 1, qualified; (ii) 74 %≤RGR≤50 %, cytotoxicity grade 2; (iii) RGR≤49 %, cytotoxicity grade 3–5, unqualified. For the cytocompatibility experiments, sterilised samples were placed into 24-well plates, and 5 × 10^4 MSCs were seeded on the samples. The proliferation of MSCs was measured at 1, 3, and 7 days via a CCK8 assay.

2.8. Animal experiments

2.8.1. In vivo implantation

All of the animal experiments were performed under a protocol approved by the Institutional Animal Care and Use Committee of Guangdong Quality Supervision and Testing Station for Medical and Health Care Appliances. Twenty-four eight-week-old male SD rats (Guangdong Quality Supervision and Testing Station for Medical and Health Care Appliances, Guangzhou, China) were used in this study and randomly divided into four groups: (1) empty defect control (blank), (2) SilMA hydrogel (Sil), (3) Exo-con/SilMA hydrogel (Sil-C), and (4) Exo-BG/SilMA hydrogel (Sil-B). A rat calvarial bone defect model was established by drilling a 5 mm diameter hole with Zoletil®50 (10 mg/kg) on both sides of the cranium. Briefly, routine skin preparation, disinfection, and towel placement were performed at the site of the defect. A lateral longitudinal incision approximately 1.5 cm in length was made in the skull. The skin and periosteum were cut layer by layer, and a cylindrical defect (diameter = 5 mm) was drilled on both sides of the cranium herringbone line via a medium-speed grinding drill. The defect was formed by rotation via haemostatic forceps, and the deep residual bone mass was removed with a small curette. The hydrogels (50 μl) were injected into the defects, and the blank group was left untreated. Blue light was applied for 30 s, and 0.5 mol/l calcium chloride solution was added for 2 min. The wounds were sutured, and a prophylactic antibiotic was administered to avoid infection.

2.8.2. Micro-CT analysis

At the end of the study period (4 and 8 weeks postsurgery), the rats were euthanised, and the calvarial bone was harvested from each rat. After fixation with 4 % paraformaldehyde for 48 h, a micro-CT instrument (ZKKS-MCT-Sharp, Guangzhou Zhongke Kaisheng Medical Technology Co. Ltd.) was used to scan the cranium samples to quantitatively analyse the newly formed bone within the defects. The sample scanning conditions were set as follows: a scanning voltage of 70 kV, a power of 7 W, 4-frame superposition, an angle gain of 0.72°, an exposure time of 100 ms, and one rotation to complete the scan.

2.8.3. Histological analysis

After being fixed with 4 % paraformaldehyde for 48 h, the cranium samples were decalcified in 10 % EDTA demineralising solution for one month. Then, 5-μm-thick sections were cut from the paraffin-embedded tissue for histological evaluation. To identify new bone formation, haematoxylin and eosin (H&E) staining and Masson's trichrome staining were performed on the sections from each sample. For immunofluorescence staining, the sections were immersed in 3 % (w/v) H_2O_2 and blocked in 3 % (v/v) BSA solution. Following enzymatic antigen retrieval, the sections were incubated with primary antibodies against BMP-2 (rat, 1:100 dilution; Abcam, USA), COLI (rat, 1:2000 dilution; Abcam, USA), VEGF (rat, 1:200 dilution; Abcam, USA), CD31 (rat, 1:2000 dilution; Abcam, USA), CD163 (rat, 1:100 dilution; Abcam, USA), and inducible nitric oxide synthase (rat, 1:2000 dilution; iNOS, Abcam, USA). After being rinsed twice with PBS, the samples were incubated with the corresponding horseradish peroxidase-labelled secondary antibodies, followed by incubation with 4',6-diamidino-2-phenylindole (DAPI) for visualisation. Nuclei were counterstained with haematoxylin. The percentage areas of iNOS, CD163, COLI, and OCN in each immunohistochemically stained sample were analysed via ImageJ. Major organs, such as the heart, liver, spleen, lungs, and kidneys, were similarly sectioned and stained with H&E via the above methods.

2.9. Statistical analysis

The experiments were repeated six times, and the results are expressed as the means ± standard deviations. All of the statistical analyses were performed with SPSS software. One-way analysis of variance (ANOVA) followed by Dunnett's multiple comparisons test was used to evaluate the significance of differences between experimental groups. The confidence interval was set at 95 %. p values < 0.05, 0.01 and 0.001 were considered to indicate statistical significance.

3. Results

3.1. Preparation and characterisation of mBG and its extracts

We prepared mBG with the sol–gel method combined with the template method, and its ionic products were obtained by immersing the mBG powder in DMEM. The physicochemical properties of the mBG, the ionic concentration of the mBG ionic products and the effects of these products on the proliferation and osteogenic differentiation of MSCs were characterised via SEM, TEM, ICP–OES, CCK-8, and ALP activity.

Fig. 1A and G shows TEM and SEM images of the prepared mBG. The results revealed that the mBG was composed of regular spherical particles with a relatively uniform size, and the dispersion between the microspheres was suitable, with no obvious agglomeration or adhesion. According to the TEM images (Fig. 1A), the brightness of the microspheres decreases towards the inside of the spheres, which is mainly due to the change in the penetration strength of the electron beam in the vertical direction when the TEM beam illuminates the surface of the microspheres. The greater natural colour excess and gradual deepening of the photographs indicate that the internal structure of the microspheres had no obvious specificity and mainly consisted of the accumulation of small nanoparticles that formed slit-shaped voids. Fig. 1B shows that the small-angle XRD pattern of the sample has a peak at 2–3 °C, which is the characteristic diffraction peak of mesoporous structure materials. Fig. 1C shows the N_2 adsorption–desorption isothermal curves and pore size distributions of the mBGs. The samples had type IV isothermal curves corresponding to mesoporous materials, which are H3-type hysteresis loops, suggesting that the samples were slit pores, which is in agreement with the results of the TEM analysis. The pore size distribution graph shows that the pores in the sample were mainly concentrated between 2 and 4 nm in size. The specific surface area of the sample was 132.9 m^2/g, the average pore size was 3.23 nm, and the pore volume was 0.0045 cm^3/g. The XPS spectra showed obvious characteristic peaks corresponding to Si, O, Ca, and P (Fig. 1D1). On the basis of the molar and mass ratios of the elements obtained from the analysis, calculations were performed to obtain the corresponding molar ratios of each element in the mBG. The corresponding molar ratio of each element in the mBG was roughly SiO_2:CaO:P_2O_5 = 89:9:2 (Fig. 1D2). To further investigate the particle size distribution and average particle size, the samples were characterised via dynamic light scattering (DLS), and Fig. 1E shows the particle size distribution of the samples. The figure shows that the particle size distribution of mBG is relatively narrow (i.e., the sample is well dispersed, with an average particle size of 649 ± 33 nm), which is consistent with the SEM and TEM observations. The average zeta potential of the sample was −12.8 ± 1.2 mV, as shown in Fig. 1F.

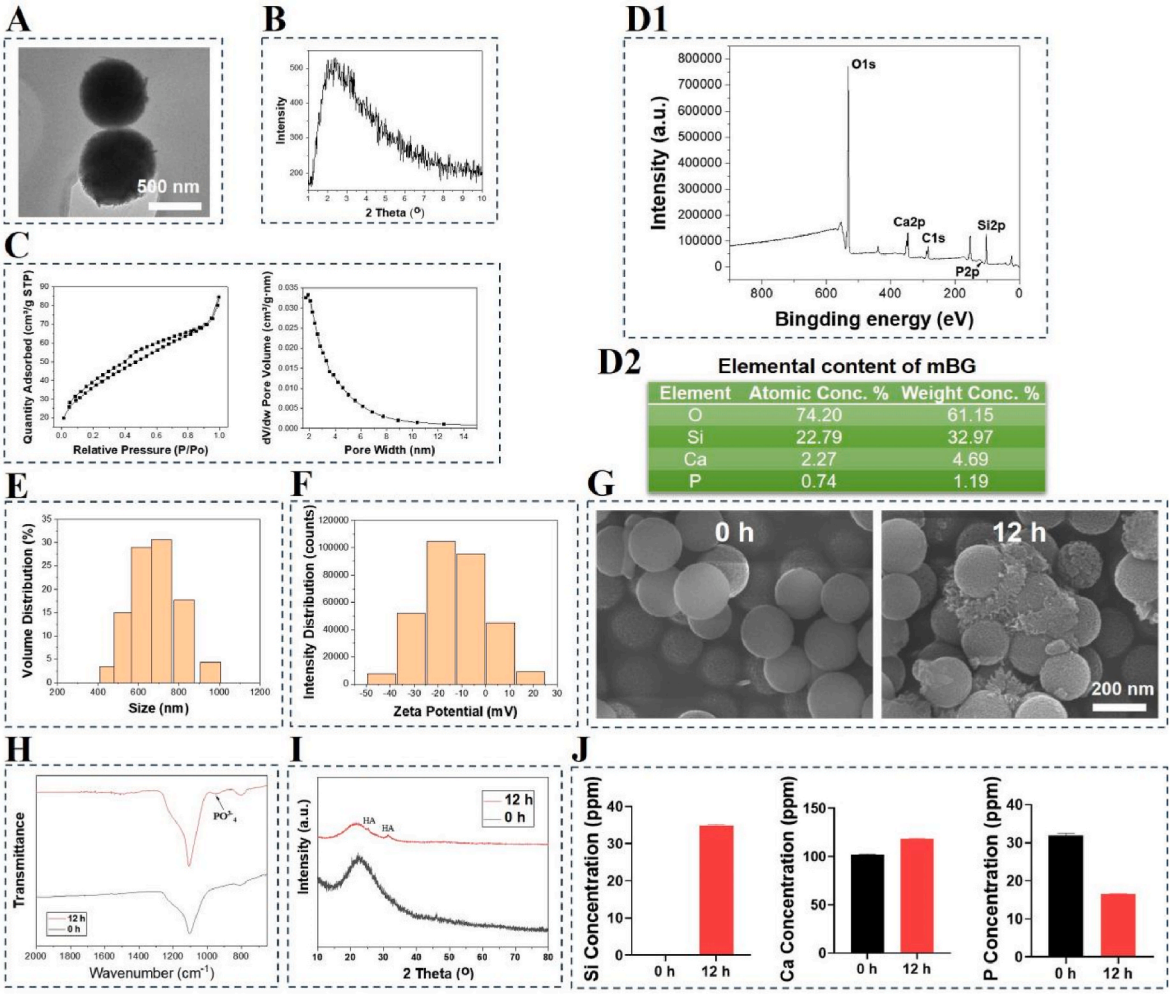

Figure 1. Characterisation of the mBG. A The mBG was shown to be composed of regular, well-dispersed nanospheres by TEM (A). B Small-angle XRD demonstrated that the BG had a mesoporous structure. C The adsorption–desorption isotherm and pore size distribution of the mBG, measured by nitrogen adsorption–desorption. D XPS spectra (D1) and corresponding elemental composition and content (D2) of mBG. E–F Particle size distribution (E) and zeta potential (F) were tested by nanoparticle size and zeta potential analysis (DLS). G–J The surface morphology determined via SEM (G), FTIR spectra (H), XRD spectra (I) and ionic concentrations of Si, Ca and P in SBF (J) before and after 12 h of immersion in SBF show that mBG can be mineralised in SBF; *p < 0.05, **p < 0.01, and ***p < 0.001.

To test the in vitro apatite formation ability of mBG microspheres, the crystalline phase composition and the intensity of the diffraction peaks of the samples after reacting in SBF for a certain period were tested via the XRD technique. As shown in Fig. 1I, the wide-angle XRD pattern of the sample had a bun peak at 15–30 °C, which is the characteristic diffraction peak of amorphous silicate material. The XRD patterns of the samples after 12 h of reaction produced new diffraction peaks at $2\theta = 26^{\circ}$ and 32°, which are the characteristic main diffraction peaks of HA (JCPDS-09-0432) (002) crystal plane and (211) crystal plane. The sample had obvious infrared absorptions at 1090 and 800 cm^{-1}, which correspond to typical Si-O-Si nonstretching vibrational peaks and Si-O symmetric stretching vibrational peaks, respectively (Fig. 1H). The P-O stretching vibration peaks of the phosphate group PO_4^{3-} were produced in the BG-mineralised samples after 12 h of reaction, which is the position referred to by the wavenumber of approximately 962 cm^{-1} in the infrared spectrum, and these infrared absorption peaks proved that apatite crystals were generated on the surface of the BG microspheres in SBF [31][Badry, 2000 #11]. Compared with the surface morphology of the BG microspheres before the reaction, the surface of the samples changed significantly after 12 h of reaction in SBF, a new deposit was generated, and the analysis of the XRD and FTIR results proved that this layer of newly formed needle-like deposits was apatite.

The change in Ca ion concentration in SBF is related to the dissolution of Ca ions from the bioglass and the formation of apatite on the surface [32]. The chemical interaction of bioactive glasses with tissues first manifests as ion solubilisation in the humoral environment, so it is necessary to study the ion solubilisation properties of bioactive glasses. Fig. 1J shows the ionic concentration changes of Si, Ca, and P after 12 h of immersion of mBG microspheres in SBF. The Si ion concentration in the solution increased rapidly after 12 h of reaction. This was due to the rapid release of free Si ions on the surface at the beginning of the immersion of the BG microspheres; the Ca ion concentration in the solution increased in the period of 0–12 h. At the beginning of the reaction of BG in SBF, the Ca ions were rapidly released, and the concentration in the solution increased. The P ion concentration of the material tended to decrease because the P ions were continuously consumed in the process of apatite deposition. The above results demonstrated that BGs with mesoporous structures were successfully prepared.

The concentrations of Ca, P, and Si in the basal medium and in the mBG ionic products were examined via the ICP–OES technique (Table 2), and the Ca concentrations in the Ctrl and mBG groups were 75.66 ppm and 70.31 ppm, respectively. The P concentration in the Ctrl group (28.75 ppm) was greater than that in the mBG group (22.88 ppm). The Ctrl group contained almost no Si (0.16 ppm), whereas the mBG group had 17.59 ppm Si.

Fig. 2A shows the proliferative capacity of MSCs cultured in mBG extract for different durations, as determined via AMPI staining and the CCK-8 method. The absorbance values of the MSCs in the Ctrl group were greater than those in the mBG group on Days 1 and 3, but the absorbance values of the cells in the mBG group were greater than those of the cells in the Ctrl group by Day 7. The results of live–dead cell staining on the third day were consistent with the results of the CCK-8 assay. These results indicate that the mBG ionic products began to significantly promote the proliferation of MSCs after 7 days of culture compared with that of control MSCs. The ability of mBG to promote the osteogenic differentiation of MSCs is an important indicator of the osteoinductive ability of mBG. Fig. 2B shows the results of ALP staining and activity quantification relative to the total protein concentration for the osteogenic differentiation of MSCs in mBG extract after 7 days. ALP activity is a key measure of the osteogenic differentiation of cells. After 7 days of culture, cells cultured with the mBG without any differentiation growth factors were found to have significantly higher ALP activity than were observed in those cultured in control conditions. The results of ALP staining were consistent with the results of activity quantification. We measured the expression of osteogenesis-related genes (ALP, Runx2, BMP2, COL1, and OPN) via qRT–PCR on Days 7 and 14, and the results are displayed in Fig. 2D. The expression of all the analysed genes was significantly upregulated in the mBG group at the two time points, with values significantly greater than those in the control group. These findings are consistent with the ALP quantification analysis and staining results obtained on Days 3 and 7, which were confirmed by Alizarin red calcium nodule staining on Day 14 (Fig. 2C); this staining is a key indicator of the late stage of osteogenic differentiation. The above results indicate that in the absence of osteogenic differentiation factors, the ionic products of mBG could effectively promote the proliferation and

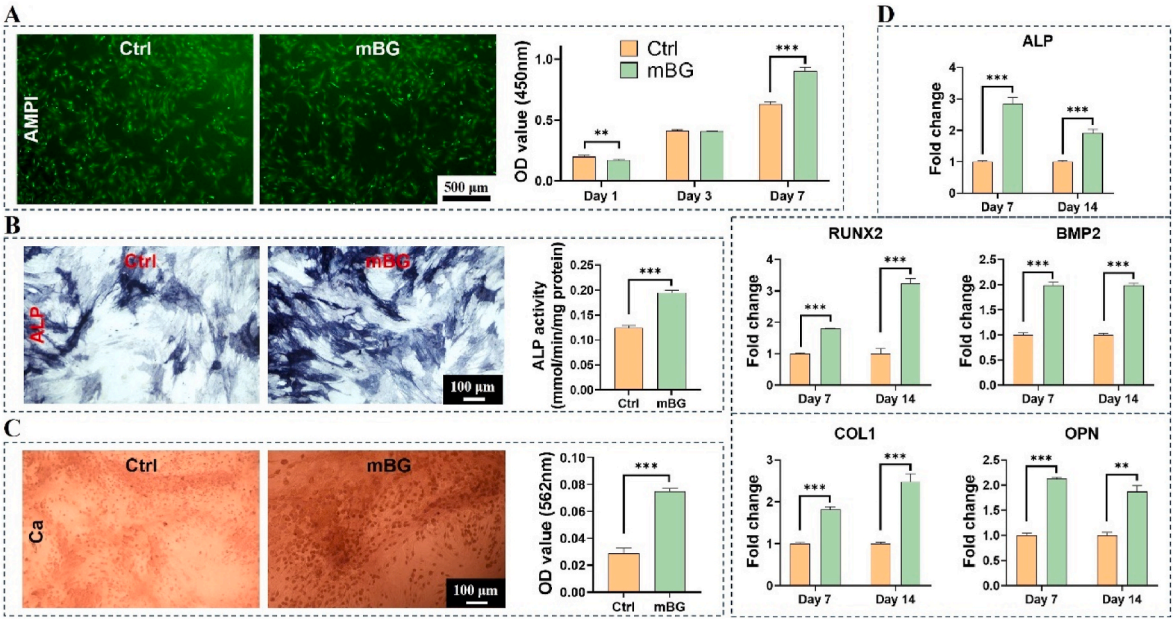

Figure 2. Cytocompatibility and osteogenic differentiation properties of the ion products of mBG. Compared with the control, the ion products of mBG promoted MSC proliferation (A, AMPI staining and CCK-8 assay) and osteogenic differentiation (B, ALP staining and activity quantification assay; C, Alizarin red staining and quantitative results of calcium nodules; D, expression of ALP, RUNX2, BMP2, COL1, and OPN osteogenesis-related genes via PCR); *p < 0.05, **p < 0.01, and ***p < 0.001.

osteogenic differentiation of MSCs.

3.2. Extraction and characterisation of MSC-derived exosomes

We used ultracentrifugation to isolate and extract exosomes secreted by MSCs and characterised their surface morphology, particle size distribution, purity, and concentration via TEM and nanoflow cytometry.

As shown in the TEM and HSFCM images, both mBG ion product-stimulated MSC-derived exosomes (mBG group) and conventionally cultured MSC-derived exosomes (Ctrl group) exhibited typical round or cup-like small membrane vesicles (Fig. 3A and B) with a size distribution of 50–140 nm and a mean size of 85.1 ± 1.5 nm and 84.8 ± 2.1 nm, respectively (Fig. 3C). In addition, the purity assessment results indicated that the percentage of vesicles among the collected MSC-derived exosomes reached 91–94 % in the two groups, demonstrating the high purity of the collected exosomes (Fig. 3D). Taken together, these findings revealed the collected vesicles as typical exosomes, and there was no significant difference between the mBG and Ctrl groups in terms of morphology, size distribution, or vesicle purity. The exosome particle concentrations in the culture supernatant were also determined with HSFCM. The exosome concentration in the mBG group was markedly greater than that in the Ctrl group (Fig. 3E). These findings indicate that the morphology, particle size and purity of the exosomes obtained after treatment of MSCs with the ionic products of mBG were similar to those of the untreated group, but the yield of the exosomes was significantly greater in the treated group.

3.3. Exo-mBG accelerates the proliferation and osteogenic differentiation of OBs

To evaluate the effects of exosomes produced by MSCs on OBs in the presence of mBG ionic products, we cocultured OBs with MSC-derived exosomes or Exo-mBGs and characterised their proliferation and osteogenic differentiation behaviours via a CCK-8 assay, ALP staining and quantification, calcineurin staining and quantification, BMP-2 immunofluorescence staining and PCR.

As shown in Fig. 4A, the absorbance values of the cells cultured with Exo-mBG were significantly greater than those of the blank culture plate group and Exo-Ctrl group at 1, 3 and 7 days. The absorbance values of the cells in the Exo-Ctrl group were also significantly greater than those in the blank culture plate group at 3 and 7 days. These results indicated that, compared with the blank control, both Exo-mBG and Exo-Ctrl significantly promoted the proliferation of OBs, and the pro-proliferative effect of Exo-mBG was the greatest.

To evaluate the osteogenic differentiation of the Exo-treated OBs in each group, we measured the expression of osteogenesis-related genes (ALP, Runx2, BMP2, COL1, and OPN) via qRT−PCR on Days 3 and 7, and the results are displayed in Fig. 4 E. The expression of most of the analysed genes was significantly upregulated in the Exo-mBG group at the two time points, with values significantly greater than those of the control group and the Exo-Ctrl groups. At several time points, such as on Day 3, the expression of the COL1 and OPN genes in the Exo-Ctrl group was significantly greater than that in the blank group, and the expression of various osteogenic genes in the Exo-mBG group was 1.05–2.67 times greater than that in the Exo-Ctrl and blank groups. By Day 7, the expression of each osteogenic gene in the Exo-mBG group was still significantly greater than that in the other two groups, and the difference in expression between the groups further increased. For example, the expression of the OPN gene in the Exo-Ctrl group was 3.97 and 2.83 times greater than that in the blank and Exo-mBG groups, respectively. OPN gene expression in the Exo-Ctrl group was also greater than that in the blank group. Alkaline phosphatase (ALP) regulates the formation of

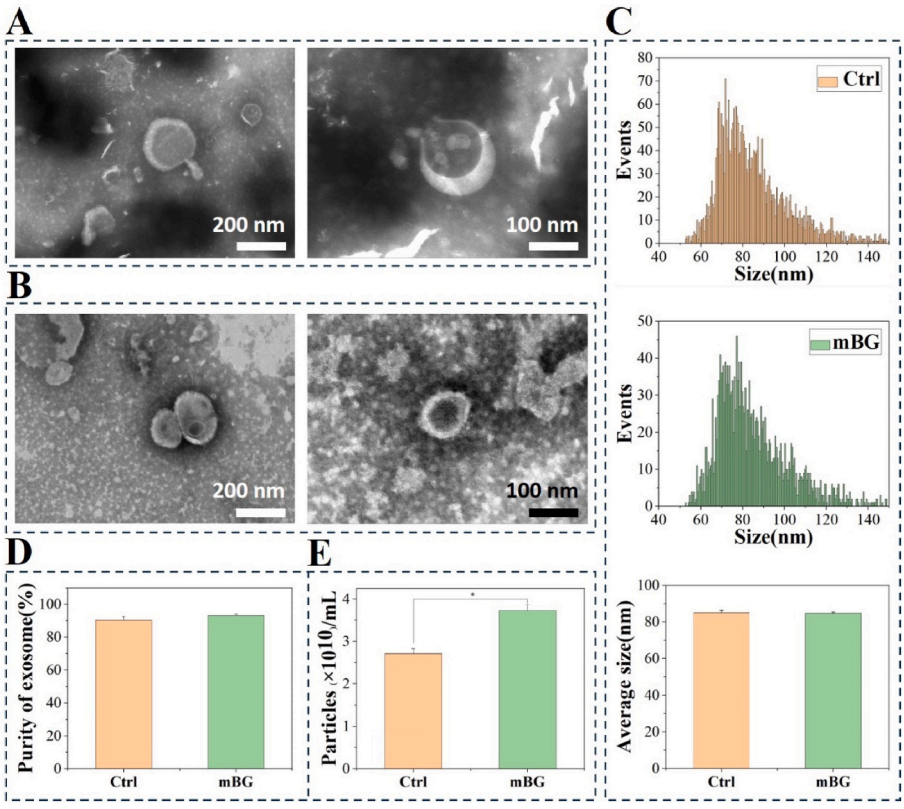

Figure 3. Characterisation of the properties of exosomes secreted by mBG-stimulated MSCs. A-B Exosomes secreted by both the control (A) and mBG groups (B) were vesicles with a diameter of approximately 85 nm according to TEM. C. Nanoflow cytometry was used to characterise the particle size distribution of the control (C1) and mBG (C2) groups as well as the average particle size (C3). D-E. Nanoflow cytometry was used to characterise the purity (D) and concentration (E) of the exosomes; *p < 0.05, **p < 0.01, and ***p < 0.001.

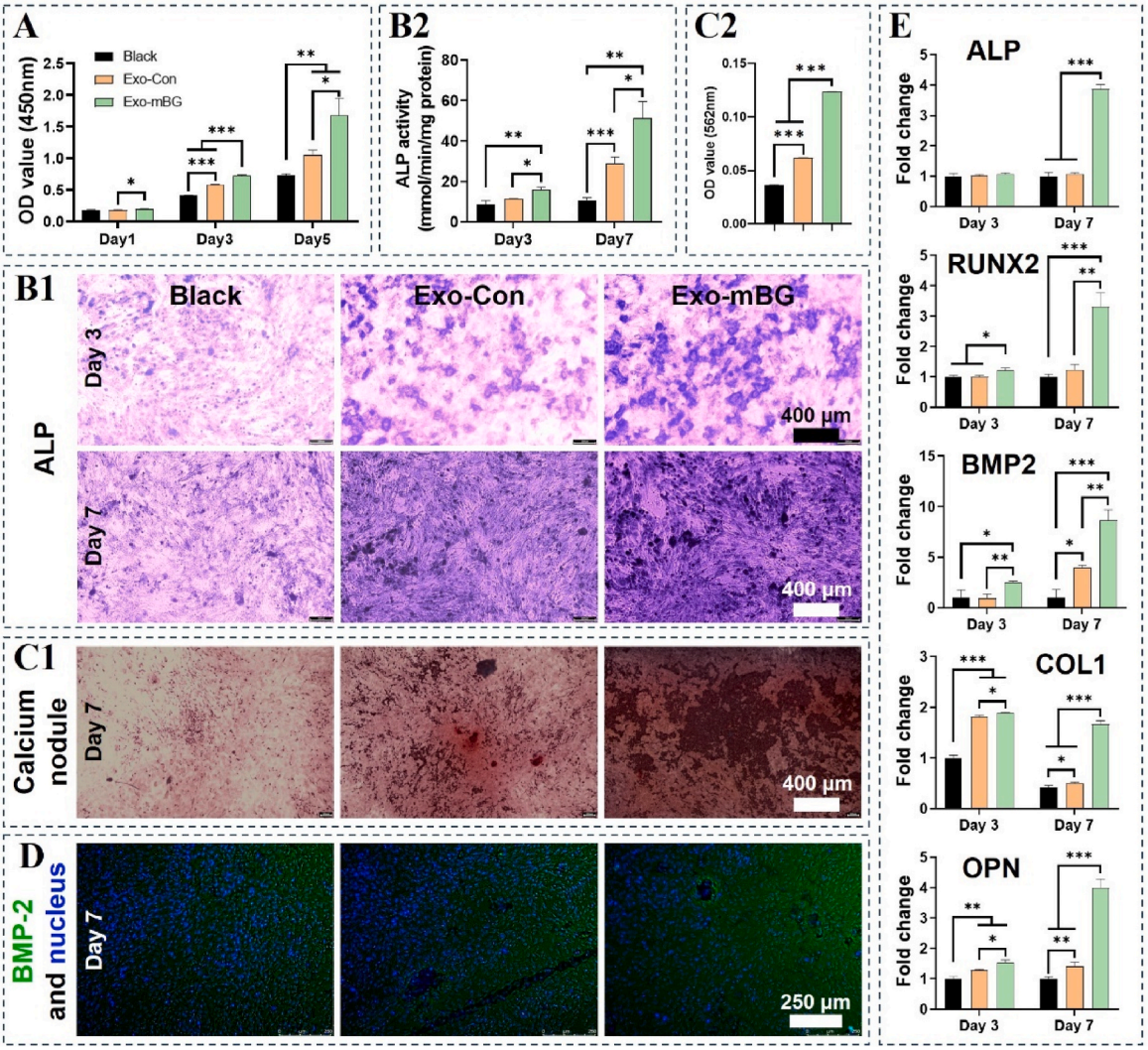

Figure 4. Effects of exosomes secreted by mBG-treated MSCs on the proliferation and osteogenic differentiation of OBs. Compared with those in the blank and control exosome groups, exosomes in the mBG group significantly promoted the proliferation of OBs. B-D Compared with those in the blank and control exosome groups, exosomes in the mBG group significantly promoted the expression of ALP (B1: ALP staining; B2: quantification of ALP activity), calcium nodule deposition (C1: calcium nodule staining; C2: calcium nodule quantification), BMP-2 expression (D: immunofluorescence staining), and the expression of ALP, RUNX2, BMP2, COL1, and OPN osteogenesis-related genes (E: PCR); *p < 0.05, **p < 0.01, and ***p < 0.001.

calcium phosphate in the extracellular matrix and is an important biomarker for early bone formation. Fig. 4 B1 and B2 show the results of ALP staining and activity quantification for Exo-mBG and Exo-Ctrl after 3 and 7 days of coculture with OBs, respectively. After 3 days of exosome and cell coculture, all of the experimental groups exhibited ALP expression; ALP expression was significantly higher in the Exo-mBG group than in the blank and Exo-Ctrl groups. After 7 days of coculture, the number of positive cells in all groups was significantly greater than that after 3 days. ALP expression in the Exo-mBG group was significantly greater than that in the blank group and Exo-Ctrl group, and ALP expression in the Exo-Ctrl group was also significantly greater than that in the blank group. The results of ALP staining were consistent with the results of activity quantification. These findings are consistent with the ALP quantification analysis and staining results obtained on Days 3 and 7, which were confirmed by Alizarin red calcium nodule staining on Day 7 (Fig. 4C1 and C2). Similarly, the change in the fluorescence of BMP-2 in all the groups was consistent with the changes observed via PCR, ALP staining, and calcium nodule analysis, so as the WB (Fig. 1S). In summary, compared with the blank and Exo-Ctrl groups, the Exo-mBG group exhibited greater OB proliferation and osteogenic differentiation in vitro.

3.4. Exo-mBG increased M2 polarisation and inhibited M1 polarisation of MPs

In this study, we cocultured exosomes produced from MSCs with p-RAW264.7 cells, and the expression levels of M1 macrophage-immunomarker genes (TNFα and IL-1β) and M2-immunomarker genes (CD206 and ARG) were detected via PCR. The expression levels of M1 and M2 type MP marker proteins (CD11c and CD206) were detected via flow cytometry. The concentrations of IL-10 and IL-12 in the culture medium were detected via ELISA kits, and the expression levels of the TNFα, IL-1β, CD206 and ARG proteins were detected via WB.

In terms of in vitro immunoregulation of the scaffolds, overall, the expression of proinflammatory genes (TNF-α and IL-1β) in the Exo-Con and Exo-mBG groups was markedly downregulated compared with that in the blank group; the greatest downregulation was observed in the Exo-mBG group (Fig. 5A). Compared with those in the blank group, the expression of CD206 and ARG was significantly upregulated in the Exo-Con and Exo-mBG groups, and the Exo-mBG group still presented the greatest change in expression (Fig. 5A). IL-10 and IL-12 protein expression in exosome-treated RAW264.7 cells was quantified via ELISA, and the results are shown in Fig. 5B. The expression of IL-10 was

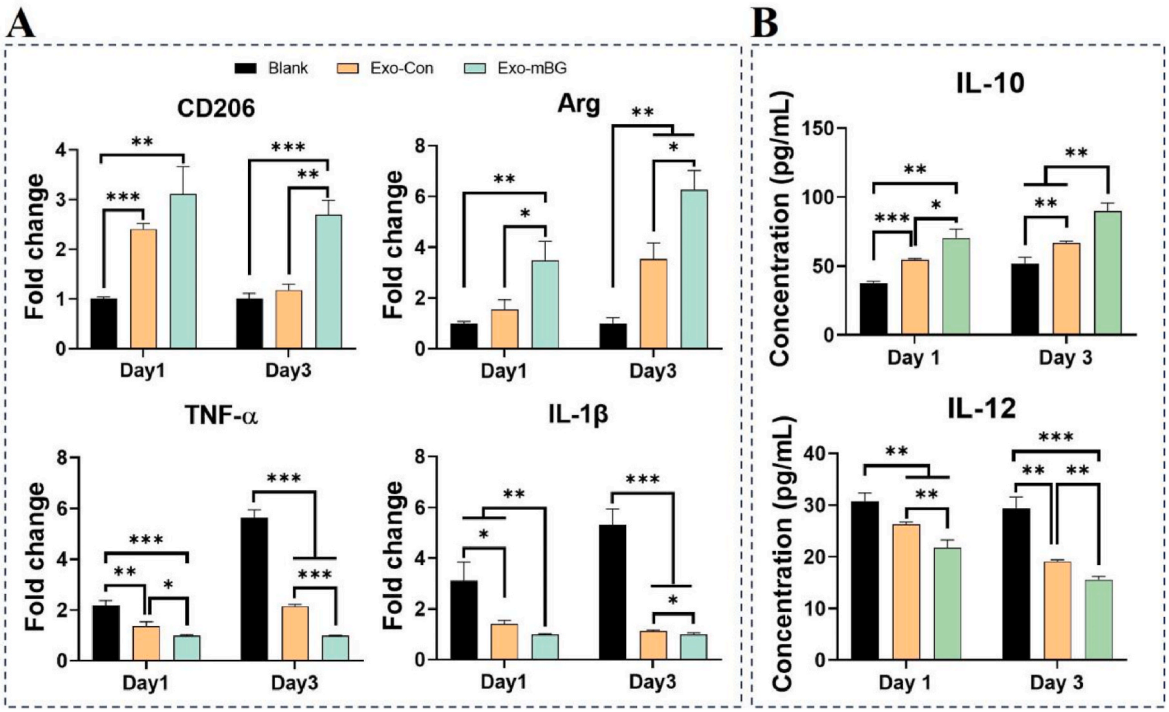

Figure 5. Effects of exosomes secreted by mBG-treated MSCs on the phenotypic polarisation of MPs, as determined by PCR (A) and ELISA (B). Compared with the blank and Exo-Con groups, the Exo-mBG group presented significantly increased M2 polarisation (CD206, Arg gene, and IL-10 protein) and inhibited M1 polarisation (TNF-α, IL-1β, and IL-12 protein); *p < 0.05, **p < 0.01, and ***p < 0.001.

significantly elevated in RAW264.7 cells treated with exosomes on both Days 1 and 3 (approximately 1.5- and 1.9-fold higher on Day 1 and 1.3- and 1.7-fold higher on Day 3, respectively), and the expression of both of these genes in the Exo-mBG group was significantly greater than that in the Exo-Con group. Compared with that in the control group, the expression of IL-12 after exosome treatment was significantly lower, and the expression of all of these genes in the Exo-mBG group was significantly lower than that in the Exo-Con group (81–83 % of those in the Exo-mBG group). Flow cytometry was also used to analyse RAW264.7 cells for one day, and the results revealed that the expression level of M2-type RAW264.7 cells in the Exo-mBG group was greater (Fig. 6A) and that there were fewer M1-type RAW264.7 cells in the Exo-mBG group than in the other groups (Fig. 6B). As shown in Fig. S2, the trend of WB results is also consistent with PCR, ELISA, and flow-through.

3.5. Exo-mBG accelerates in vivo bone reconstruction and regeneration

To study the effect of Exo-mBG on bone repair, we established a skull defect model in Sprague–Dawley (SD) rats. We chose SilMA, which can be injected in situ and light-cured, as the carrier material for exosomes. A sham operation group (blank), a material control group (SilMA, named the Sil group), and two experimental groups (Exo-con/SilMA and Exo-mBG/SilMA, named the Sil-C and Sil-B groups, respectively) were established. Micro-CT imaging and H&E, Masson's trichrome and immunofluorescence staining (for BMP2, COL1, VEGF, CD31, CD163, and iNOS) were used to systematically evaluate bone tissue repair, angiogenesis and the immune response of macrophages.

Moreover, the cytotoxicity and cytocompatibility of exosome-containing SilMA using OBs and MSCs were investigated. The cytotoxicity was grade 0 for the negative control, Sil, Sil-C and Sil-B and grade 5 for the positive control (Table S1). As shown in Fig. S3, the OD values of MSC proliferation in each group increased with increasing incubation time. On day 1 of coculture, the OD values of the blank group were significantly lower than those of the other three groups, whereas the differences among the remaining groups were not significant. On day 3, the OD values of the exosome-containing Sil group were significantly greater than those of the blank and Sil groups. On day 7, the OD values of the groups decreased in the order of Sil-B, Sil-C, Sil, and Blank, and there was a significant difference among all the groups. The results showed that exosome-containing SilMA was not cytotoxic or biocompatible. In parallel, we evaluated the exosomal release behaviour of SilMA in vitro. The SilMA-loaded exosomes in both groups were released rapidly in the first week, followed by slow-release rates of 81.12 % and 83.09 % on Day 28 in the Sil-C and Sil-B groups, respectively (Fig. S4).

As shown in Fig. 7A, at 1 and 2 months after surgery, representative micro-CT images of the defect site were similar and consistent with the in vitro osteogenic differentiation results. At 1 month, within the defect site, new bone formation was significantly greater in the Sil-B group than in the other groups. Calcification and bone tissue formation further increased in the experimental group at 2 months, but the blank group still had large bone defects with no signs of bone healing. The control and experimental hydrogel groups presented increased growth of bone tissue from the periphery to the centre of the defect site over time. Quantitative analysis of the relevant micro-CT parameters confirmed this trend (Fig. 7B–F). At 1 and 2 months, the bone volume fraction (BV/TV) and bone mineral density (BMD) data revealed that the amount of new bone was significantly greater in the Sil-B group than in the other three groups, whereas the amount in the Sil-C group was greater than that in the blank group. Among the main indices of bone trabecular space morphology, trabecular thickness (TB.th) and trabecular number (TB.N.) increased in all groups, whereas trabecular separateness (TB.Sp) decreased in all groups, which was consistent with our expectations.

To further evaluate the presence of new bone at the interface of the hydrogel and the bone defect, we performed histological staining after 1 and 2 months (Figs. 8 and 9). The H&E staining results revealed that after 1 month, compared with the other two groups, the Sil-B group presented a thicker layer of lamellar collagenous fibrous tissue, with a central canal and a rich distribution of striated blood vessels. In contrast, the Sil, Sil-C and blank groups had a thinner layer of connective tissue, predominantly comprising collagen fibres. However, the Sil-C group had

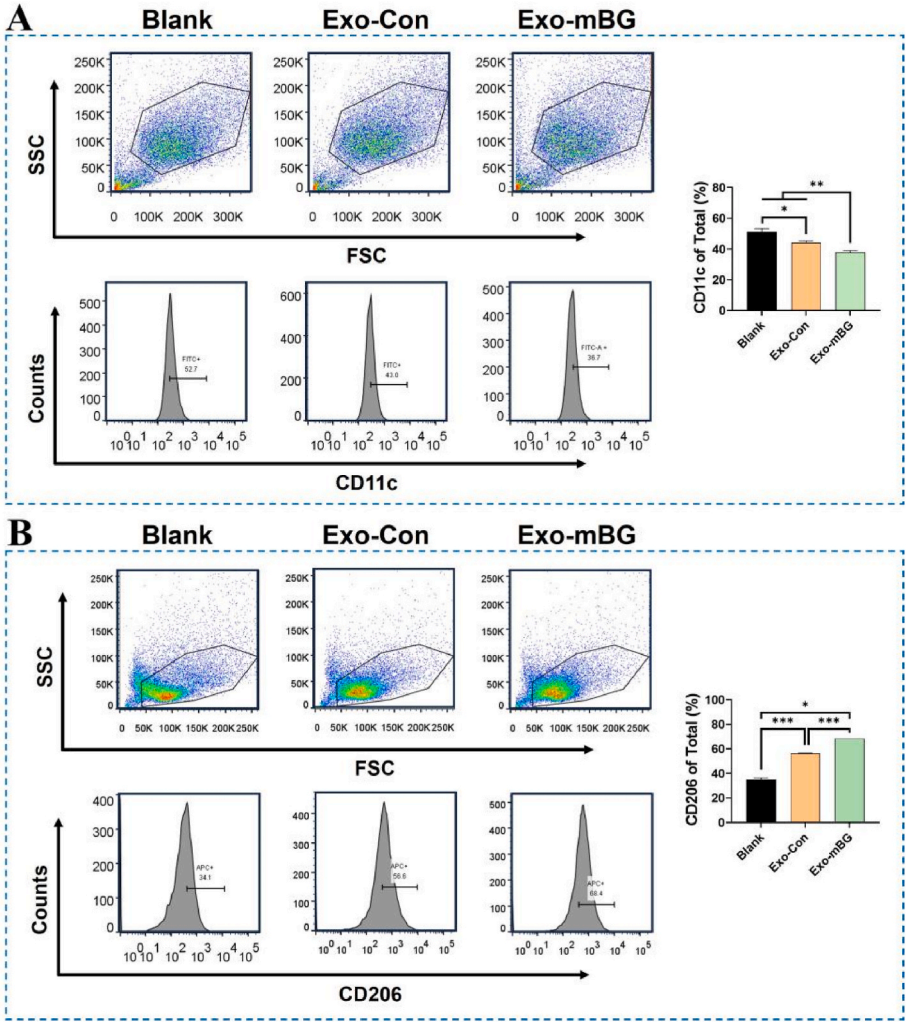

Figure 6. Flow cytometry analyses and statistics of CD11c (A) and CD206 (B) expression in RAW264.7 cells after 1 day. Compared with those in the blank and Exo-Con groups, the Exo-mBG group presented significantly more protein markers of the M2 type (CD206) and fewer protein markers of the M1 type (CD11c); *p < 0.05, **p < 0.01, and ***p < 0.001.

a thicker and more mineralised lamina, and the blank group had an uneven distribution of thick and thin neoplastic tissue, with fewer vascular shadows. The results of Masson staining were consistent with the results of H&E staining, as shown in Fig. 8. Dark blue indicates mature bone tissue, light blue indicates fibrous connective tissue, and red indicates myofibrillar tissue. After 1 month, the bone defects were mainly filled with fibrous connective tissue, but the connective tissue in the Sil-B group was thick and dense, with many red-stained blood vessel walls within it, and the remaining two groups had relatively sparse connective tissue. Immunofluorescence staining for BMP-2, Col1, CD163, iNOS, VEGF and CD31 was performed after 1 month to evaluate osteogenesis, angiogenesis and the immune response at the defect site. The results are also shown in Fig. 8. Compared with those in the other groups, the Sil-B group exhibited significant deposition of the Col1 and BMP-2 proteins at the defect site, indicating that the Sil-B group had better osteogenic effects, which was consistent with the micro-CT, H&E staining, and Masson staining results (Figs. 7–9). Moreover, macrophage polarisation plays an important role in the quality and efficiency of bone repair in organisms. The M1 phenotype appears during the early stage of inflammation and recruits many inflammatory cells to induce inflammation, which affects the healing outcome, whereas the M2 phenotype promotes both angiogenesis and tissue repair, allowing the tissue to return to its original state. Notably, the expression of the stimulated macrophage M2 marker CD163 was significantly greater in the Sil-B group than in the other three groups, while the expression of the macrophage M1 marker iNOS was significantly lower, which suggests that Sil-B can most strongly modulate the conversion of macrophages from the M1 phenotype to the M2 phenotype in vivo. Unexpectedly, the Sil-B combination had the greatest effect on the expression of proangiogenic factors, with the highest VEGF and CD31 expression levels, followed by the Sil-B, Sil and blank groups.

This trend was also observed at 2 months via H&E staining (Fig. 9), with further ossification of the neoplastic tissue in all four groups, and the neoplastic bone tissue in the Sil-B group tended to be tightly bound to the host native bone. The results of Masson staining were also consistent with the results of H&E staining. After 2 months, the fibrous connective tissue had formed mature bone tissue, the new bone at the defect site after the implantation of Sil-C was tightly connected to the native bone under the guidance of the material, and the Sil-B treatment had the greatest osteogenic effect. These results suggest that Exo-mBG-functionalised SilMA hydrogels can effectively induce in situ bone tissue regeneration without the addition of exogenous seed cells or growth factors. Immunofluorescence staining for OCN, Col1, CD163, iNOS, VEGF, and CD31 was performed again after 2 months (Fig. 9). Compared with the other groups, the Sil-B group exhibited significant deposition of the Col1 and BMP2 proteins at the defect site, indicating that the Sil-B group had better osteogenic effects, which was consistent with the micro-CT, H&E staining, and Masson staining results (Figs. 7 and 9). The

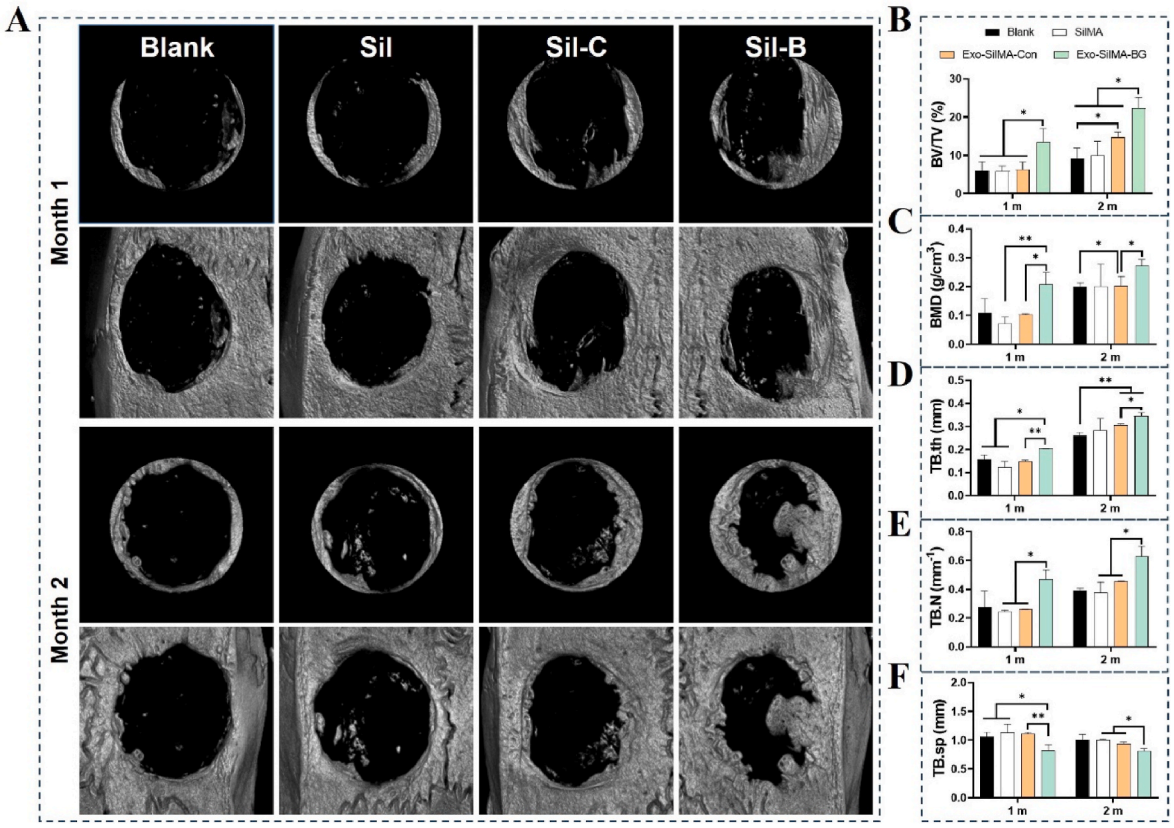

Figure 7. Effects of exosomes secreted from mBG-treated MSCs on the regenerative repair of cranial bone defects in rats, as determined via micro-CT technology. Compared with the blank, Sil and Sil-C groups, the Sil-B group significantly promoted bone regeneration at the cranial defects at both the 1st and 2 nd months after surgery (A: micro-CT 3D reconstruction image; B: new bone volume fraction; C: bone mineral density; D: trabecular thickness; E: trabecular number; F: trabecular separation); *$p < 0.05$, **$p < 0.01$, and ***$p < 0.001$.

Sil-B group also exhibited significant upregulation of the expression of the stimulated macrophage M2 marker CD163, while the expression of the macrophage M1 marker iNOS was significantly downregulated. Additionally, VEGF and CD31 were the most highly upregulated genes in the Sil-B group. This trend is consistent with the results of the first month. The results of the above animal experiments revealed that, compared with the other three groups, the Sil-B group effectively promotes bone formation and vascular regeneration, exerts strong immunoregulatory effects, induces macrophage polarisation in the M2 direction, and inhibits M1 polarisation. The area percentage results of BMP-2, COLI, VEGF, CD31, CD163, and iNOS in immunohistochemical staining sections at 1 and 2 months were consistent with those of the immunofluorescence staining images (Fig. S5).

Finally, there was no significant difference in H&E-stained sections of major organs (heart, liver, spleen, lungs, and kidneys) between the experimental rats in each group and the control rats (Fig. 10). This finding suggested that, in vivo, hydrogels containing exosomes possess suitable biocompatibility.

In summary, the results of this study indicate that the exosomes secreted by mBG ionic product-treated MSCs can promote the osteogenic differentiation of OBs in vitro and the regeneration of bone and blood vessels at bone defects in vivo, promote M2 macrophage polarisation of the MPs and inhibit M1 macrophage polarisation, which is more conducive to the regenerative repair of bone tissue.

4. Discussion

Exosomes produced by MSCs are proangiogenic and are considered a new promising and effective alternative to cell therapy for the treatment of bone defects. However, their practical application is severely limited by the difficulty of large-scale exosome production. Moreover, understanding how to improve the ability of exosomes to ameliorate tissue defects is a current research hotspot in different fields. For example, improving the function and efficiency of exosomes has been a popular research topic in the field of orthopaedics. In this study, we prepared mBG microspheres and their ionic products to treat MSCs and obtained exosomes via differential ultracentrifugation. Compared with the other groups, the Exo-mBG group significantly promoted the proliferation and osteogenic differentiation of OBs, increased bone and vascular regeneration at cranial defects in vivo, promoted M2 macrophage polarisation, and inhibited M1 polarisation. Moreover, Exo-mBG alleviated local immune inflammation, promoted vascularisation, and promoted in situ bone regeneration.

Biomaterials can act directly on cells or alter the microenvironment in which they are located to affect their growth and exosome secretion [19,22,33]. mBG is a suitable tissue regeneration biomaterial with both osteoconductive and osteoinductive properties. Compared with 45S5 BG and SBG, mBG has a nanoporous structure and a high specific surface area, can dissolve ions faster and form apatite in vitro, and has a promising future for clinical application [34,35]. There are almost no reports on the ability of mBG ionic products to improve the osteoinductive regeneration of MSC-derived exosomes in vitro or in vivo. In this study, mBG was synthesised via DDA as a catalyst for the hydrolysis of TEOS and as a templating agent for vitreous sol. During synthesis, DDA was dissolved in an aqueous alcohol solution, which rendered the solution alkaline and catalysed the hydrolysis and condensation of TEOS, resulting in the conversion of the vitreous sol into a vitreous gel. In addition, DDA consists of hydrophilic end amine groups as well as hydrophobic end long-chain alkane groups. The hydrophilic end is adsorbed on the surface of the glass precursor particles that have been

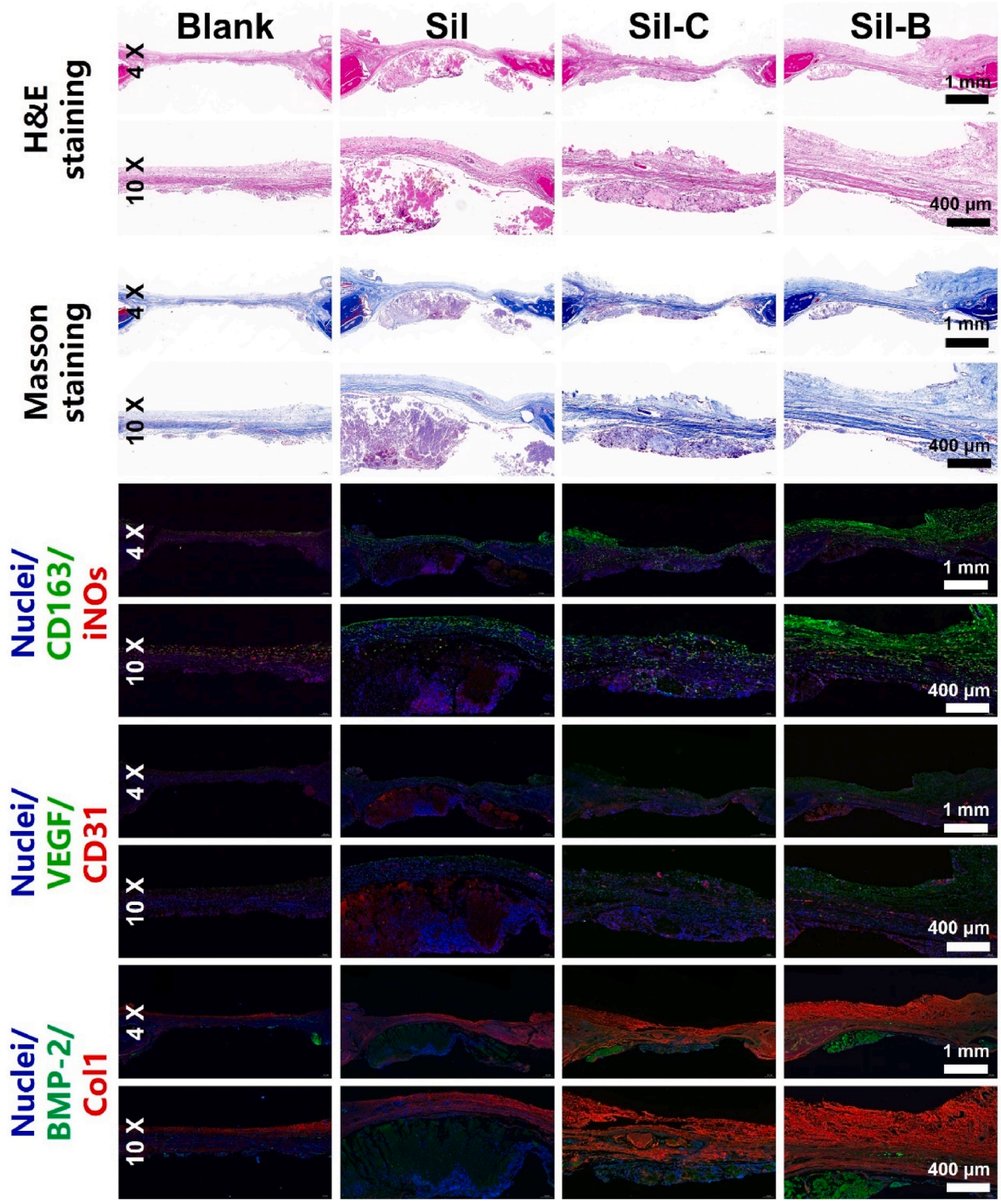

Figure 8. Effects of exosomes secreted from MSCs treated with mBG on the regenerative repair of cranial bone defects in rats 1 month after surgery, as determined via tissue section staining. Compared with the blank, Sil, and Sil-C groups, the Sil-B group presented significantly promoted bone regeneration at the cranial defects at 1 month after surgery (H&E staining and Masson staining). Moreover, the Sil-B group presented increased expression of the osteogenic-associated proteins BMP-2 (green) and COL1 (red), the vasculogenic-associated proteins VEGF (green) and CD31 (red), and the M2-type macrophage protein CD206. In contrast, the Sil-B group presented downregulated expression of the M1-type macrophage protein iNOS (red).

converted into gels, and the hydrophobic end is directed to the solution. In addition, owing to the action of the hydrophobic end groups on the surface of the glass gels, these glass gels self-assemble to form negatively charged, well-dispersed, globular particles with a particle size of 649 ± 33 nm (Fig. 1E–F) [36]. SEM and TEM images and N_2 adsorption–desorption isothermal curves revealed that the pore morphology of the mBG consisted of slit-shaped voids formed by the accumulation of fine particles (with an average pore size of 3.23 nm), which had suitable granularity (Fig. 1A–C, G). The crystal characteristics, mesopore structure, elemental content and chemical composition of the mBG were further confirmed by XRD, XPS and FTIR (Fig. 1B–D, H-I). All of these results demonstrated that BG with a mesoporous structure was successfully prepared. The chemical composition of mBG was very different from the designed chemical composition because during the synthesis of mBG, the hydrolysis and condensation of TEOS were first catalysed by DDA, which resulted in the formation of a denser reticulated Si-O

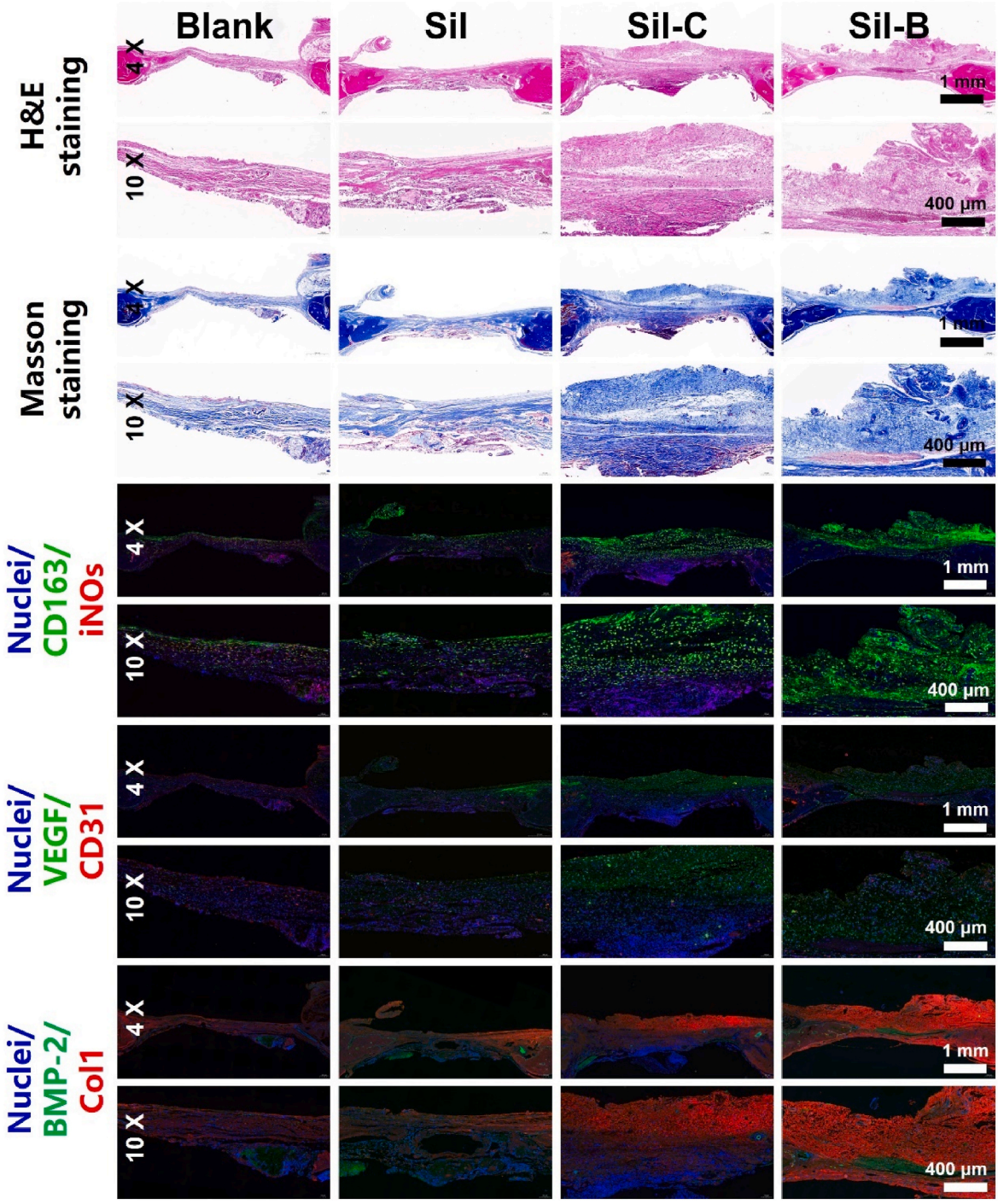

Figure 9. Effects of exosomes secreted from mBG-treated MSCs on the regenerative repair of cranial bone defects in rats at 2 months after surgery, as determined via tissue section staining. Compared with the blank, Sil, and Sil-C groups, the Sil-B group presented significantly greater bone regeneration at the cranial defects at 2 months after surgery (H&E staining and Masson's trichrome staining). Moreover, the expression of the osteogenesis-related proteins BMP-2 (green) and COL1 (red), the expression of the angiogenesis-related proteins VEGF (green) and CD31 (red), and the expression of the M2-type MP protein CD206 were increased in the Sil-B group. In contrast, the expression of the M1-type MP protein iNOS (red) was downregulated in the Sil-B group.

network under alkaline conditions, whereas TEP, the precursor of P_2O_5, which has poor water solubility, was hydrolysed more slowly under alkaline conditions, and it was difficult for the unhydrolysed TEP to remain in the Si-O network [37]. Ca in calcium nitrate appears in the reaction system in the form of Ca^{2+}, which is mainly adsorbed on the surface of the particles by electrostatic action and gradually diffuses into the network during subsequent heat treatment [38]. As a result, most of the P and Ca precursors remained in solution after the reaction, and these P and Ca raw materials were removed during centrifugation, resulting in a large difference between the actual composition and the designed composition. The ions released by BG can enhance the cellular response to glass microspheres. Moreover, these ions can activate multiple osteogenesis-related signalling pathways and recruit bone progenitor cells, which can in turn promote the entry of related transcription factors into the cell nucleus, which can bind to the promoters or enhancers of downstream genes, thus upregulating

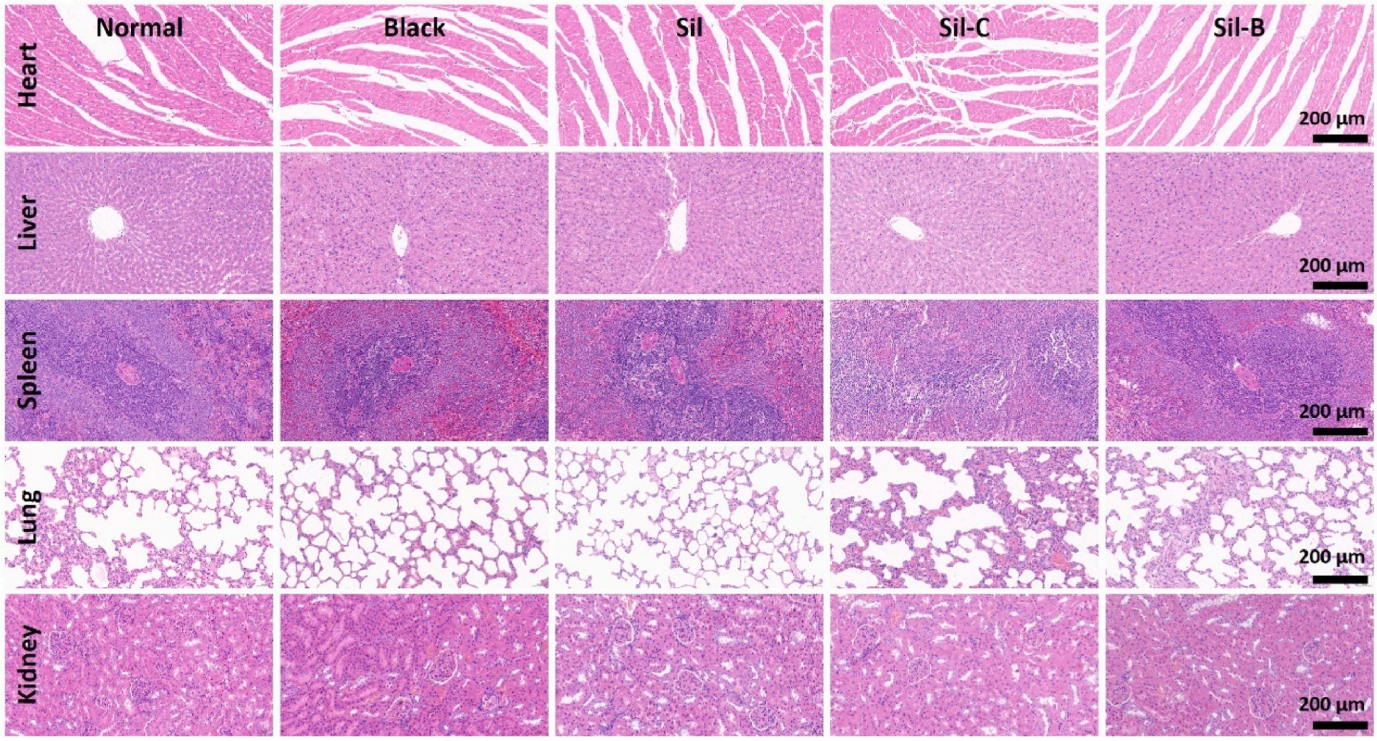

Figure 10. Histocompatibility evaluation of exosomes secreted by mBG-stimulated MSCs after 2 months of implantation on the basis of H&E staining. There were no significant differences in H&E staining of the heart, liver, spleen, lungs or kidneys between the experimental groups and the control group, demonstrating that the hydrogels had suitable biocompatibility.

osteogenesis-related genes, facilitating OB proliferation, and promoting bone mineralisation [39].

The change in ion concentration in SBF may be related to the loss of ions by material-induced apatite deposition, which is caused by the exchange of ions dissolved from the solution with the mBG (Fig. 1G–J). When the mBG is immersed in SBF, the calcium on the mBG surface, as a modifier of the glass network, is rapidly dissolved, and the dissolved Ca ions are exchanged with the H ions from the SBF. On the one hand, the nonbridging oxygen in the mBG that interacts with the calcium ions binds to the exchanged hydrogen ions, resulting in the formation of a Si–OH silica-rich gel layer on the surface of the mBG; on the other hand, owing to the exchange of the Ca ions released from the bioglass with the H ions from the solution, a Si–OH-rich gel layer is formed on the surface of the mBG. As the hydroxide concentration in the solution increases, the concentrations of Ca^{2+} and OH^- in the SBF reach supersaturation near the surface of the material and then interact with PO_4^{3-} in the SBF and PO_4^{3-} dissolved in the mBG; subsequently, the hydroxyapatite mineralised layer is formed with the surface of the mBG as the nucleation site. At the beginning of the mineralisation reaction, the Ca ion release rate of the material is faster than that of apatite deposition, so the Ca ion concentration in the solution during the first 12 h of the reaction increases, whereas P is used as a byproduct of glass network formation, and the release rate of P ions is slower than that of apatite deposition from the beginning of the mineralisation reaction. Thus, the P ion concentration in the SBF shows a decreasing trend. In contrast, the Si ion concentration in the solution shows an increasing trend because SiO_3^{2-} dissolved from mBG does not participate in the apatite deposition process [40].

Increasing the yield of exosomes produced by MSCs is a current research focus. EVs are a class of micro- and nanovesicles with a double-layer membrane structure that are secreted and released by cells during normal physiological processes and participate in cell–cell signalling [41,42]. When cells are in a metabolically active state, the EVs for intercellular transmission are predominantly exosomes. Cellular exosomes are a type of EV that are 40–200 nm long and carry many characteristic proteins of their donor cell origin. The main function of exosomes is to encapsulate and protect the signalling material secreted by the cell so that it can pass through the complex and variable extracellular environment and reach the target cell successfully [43]. In this study, exosomes produced by MSCs in a microenvironment containing mBG ion products were successfully isolated and extracted via ultracentrifugation, and the resulting exosomes were highly pure (Fig. 3 D). Moreover, exosomes secreted by MSCs under conventional culture conditions were also separately extracted via the same method to facilitate comparison. Routine evaluation of exosomes is necessary before quantitative comparisons and functional studies of exosomes can be performed. The mBG group contained slightly more large vesicles than the Ctrl group did, probably because the exosomes secreted by MSCs via mBG ionic products carried more abundant membrane proteins, which resulted in a slightly larger size in the mBG group (Fig. 3C) [44]. Treatment of MSCs with mBG ion products increased exosome production by approximately 1.4-fold compared with that of MSCs cultured in conventional serum-free culture conditions without altering the conventional vesicle characteristics of the exosomes, including morphology, purity, or size distribution (Fig. 3). In addition, cells have a greater ability to secrete and release exosomes in the absence of serum starvation or in a state of inflammatory stimulation [45,46]. Therefore, in the present study, MSCs were cultured in serum-free medium for 24 h before exosome collection.

After the recipient cell captures the exosome, many of its behaviours are modified according to the internal contents of the exosome [47,48]. When exosomes contain different types or levels of endosomes, the adjustments they make to the behaviour of receptor cells can markedly differ. The main functional cell type evaluated in this study was OBs. OBs are the main functional cells involved in bone formation in vivo and are also responsible for the synthesis, secretion, and mineralisation of the bone matrix to form bone tissue. In a comparative study, Kim et al. reported that OBs were biologically active in vitro and that they were

capable of repairing cranial bone defects in nude mice when implanted in vivo in combination with scaffolding materials [49]. Zhu et al. reported that the osteogenic capacity of these cells was much greater than that of alveolar osteoblasts and bone marrow stromal stem cells [50]. OBs are responsible for bone repair and remodelling and have long been used as classical seed cells in bone tissue engineering research. OBs and osteoclast precursor cells form mineralised nodules in vitro, which is consistent with their function in vivo. The nodule contains a collagenous matrix calcified by OBs and osteoclasts, allowing the in vitro cell culture environment to better mimic the reaction between biomaterials and bone tissue in vivo [51]. Our results revealed that when the exosome concentration was the same, MSC-derived Exo-mBG significantly promoted OBs to secrete more ALP, BMP2, and calcium nodules and to express and synthesise higher levels of functional genes and proteins closely related to osteogenesis, such as ALP, RUNX2, BMP2, COL1, and OPN, in vitro (Fig. 4 and Fig. S1). ALP is the most widely recognised early phenotypic marker of osteogenesis. Runx2 is an important osteogenic transcription factor that binds to the osteoblast-specific cis-acting element (OSE2) in the promoter region of the osteogenic gene. BMP-2 can induce the directed differentiation and proliferation of undifferentiated MSCs into chondrocytes and OBs, promote OB differentiation and maturation, and participate in bone and cartilage growth and development as well as their reconstruction process, thus accelerating bone defect repair [52]. Col-I is an extracellular matrix protein that stimulates osteoblast adhesion and differentiation [53]. OPN is one of the more abundant noncollagenous proteins in the bone matrix produced by OBs and osteoclasts and can effectively stimulate the osteoclastogenic and resorptive activity of mature osteoclasts involved in bone remodelling [54]. Calcium nodule deposition is one of the hallmarks of bone maturation [55]. These findings suggest that MSC-derived exosomes have a greater ability to promote the osteogenic differentiation of OBs in the presence of mBG ion products. To further verify the in vivo osteogenic properties of the exosomes, we created a rat skull bone defect model for in vivo experiments. In the animal experiments of this study, we used injectable and in situ light-cured SilMA hydrogels as exosome-loaded materials that could release exosomes for more than 1 month. The loading strategies employed for exosome-loaded scaffolds usually include solution adsorption and hydrogel encapsulation [56–60]. Solution adsorption methods usually result in burst release of exosomes [57,58], which can be ameliorated by chemical modification of the scaffold surface [56]. Among them, SilMA hydrogel encapsulation can provide stable sustained release while the material degrades and can be used for the regeneration of bone defects for repair [59]. Micro-CT results revealed that, as a filler material for bone defects, SilMA containing Exo-mBG was able to guide bone mineralisation from the periphery to the centre. In both the 1st and 2 nd months, the amount of new bone and the density and thickness of the bone trabeculae were significantly greater in the Sil-B group than in the blank, Sil, and Sil-C groups (Fig. 7). According to the H&E staining and Masson staining results, the Sil-B group had thicker lamellar fibrous connective tissue and was rich in internal striated blood vessels (Figs. 8 and 9). This finding indicated that the hydrogel containing Exo-mBG had significantly stronger osteogenic and angiogenic effects than the other treatments did. During bone regeneration, the immunomodulatory capacity of grafts can facilitate the induction of osteogenic and angiogenic microenvironments [61]. Moreover, iNOS and CD163, which are M1 and M2 macrophage markers, respectively, can be used to assess the polarisation of macrophages during bone repair, whereas the expression of angiogenesis-related genes, such as VEGF and CD31, can be used to assess vascularisation and osteogenesis [62,63]. As shown by the PCR, WB results and immunofluorescence images (Figs. 4, 8-9, S1, S5), the Sil-B group exhibited substantial accumulation of osteogenesis-related proteins (BMP2 and Col1) at the defect site. In terms of immunomodulatory ability, the expression of the macrophage M2 marker CD163 was significantly upregulated, whereas that of the macrophage M1 marker iNOS was significantly suppressed, further suggesting that Sil-B (Exo-mBG) has a greater ability to promote the polarisation of macrophages from the M1 phenotype to the M2 phenotype than the other two treatments do, forming an immune microenvironment enriched with M2-type macrophages, which play a positive role in the early stage of bone repair. These behaviours can alleviate inflammation during the early stage of bone repair and promote the transition of bone healing from the inflammatory phase to the healing phase [64,65]. Gaoran Ge et al. reported that the adsorption of EVs on the surface of dopamine-coated titanium implants inhibited M1 macrophages around the prosthesis, resulting in satisfactory long-term osseointegration. Reducing the formation of significantly proinflammatory M1 macrophages and promoting the formation of inflammation-suppressive M2 macrophages promotes surface osteogenesis and ultimately results in good osseointegration [66]. We observed similar results in both in vivo and in vitro experiments, i.e., the addition of MSC-derived exosomes to either the culture medium or to SilMA significantly promoted M2 macrophage formation while inhibiting M1 macrophage formation (Figs. 5–6, 8-9, S2, S5). Moreover, in vivo, MSC-derived Exo-mBG promoted vascular tissue neovascularisation to a significantly greater extent than MSC-derived Exo-Ctrl did. Vascularisation is an important process in bone defect repair and is a key factor affecting bone repair and remodelling [67]. Wang et al.'s team demonstrated that exosomes secreted by human induced pluripotent stem cell-derived MSCs can be used to enhance vascularisation in many tissue injuries, such as limb ischaemia, cutaneous wound healing, critical-sized bone defects and femoral head necrosis, by promoting angiogenesis [68–70]. Studies have also shown that an immune microenvironment enriched with M2-type macrophages favours angiogenesis during bone regeneration, which was supported by the significant VEGF and CD31 staining in immunofluorescence assays at months 1 and 2 in the Sil-B group [71]. In summary, the Exo-mBG constructed in this study robustly promoted osteogenesis and provides new ideas for developing bone grafting materials. Finally, H&E-stained sections of the heart, liver, spleen, lung, and kidney of the experimental rats one month after hydrogel implantation were not significantly different from those of the normal rats, verifying that the scaffolds were also biocompatible in vivo (Fig. 10). These results indicate that the exosomes secreted by MSCs treated with mBG ionic products can promote the osteogenic differentiation of OBs in vitro and promote bone healing and vascular regeneration in bone defects in vivo; additionally, these cells have immunomodulatory functions that also promote the regeneration and repair of bone tissues, which can regulate the secretion of exosomes and improve their practical application in the field of bone repair. In the present study, mBG was tested for its ability to regulate exosome secretion and improve its practical application in bone repair. The largest difference between the concentrations of Ca, P and Si ions was the Si concentration between the mBG group and the Ctrl group, with the mBG group exhibiting a greater concentration. The Ca and P concentrations in the mBG group were lower than those in the Ctrl group (Table 2). This significant decrease in the concentrations of Ca and P is due to the in vitro mineralisation that occurs during the immersion of mBG in DMEM [72]. In vitro experiments have demonstrated that when BG is cocultured with OBs, calcium and silicon ions dissolved in BG can promote the production of extracellular collagen and thus the formation of calcified nodules [73]. When mBG ionic products were used for coculture with MSCs, cell proliferation was inhibited in the mBG group at the initial stage, during which time cell proliferation improved (Fig. 2A). The main reason for this difference may be that the ion concentration in the solution was high at the initial stage, which was not favourable for rapid cell proliferation. When the treatment time was further prolonged, the cells adapted to the microenvironment and exhibited excellent promotion of cell proliferation with suitable cytocompatibility, which was consistent with the findings of previous reports [74]. Therefore, in the present study, MSCs were treated with normal medium or mBG ionic products for 7 days before being replaced with serum-free medium to collect the exosomes. In addition, the osteogenic differentiation of MSCs was significantly

enhanced after culture with mBG ionic products (Fig. 2B–D), indicating that the mBG ionic products promoted the osteogenic differentiation of MSCs, which was consistent with the findings of previous reports [75,76]. Moreover, the bioactivity of the mBG ion products may be derived mainly from Si ions. Si ions have been reported to significantly increase bone marrow stromal cell proliferation, mineralised nodule formation, bone-related gene expression and bone matrix protein expression [77,78]. It has also been reported that Ca and Si ions synergistically promote cell differentiation and collagen production via the TGF pathway [79]. Ding et al. reported that silicate ions released during the degradation of calcium silicate bone cement can promote cell proliferation and stimulate the expression of bone-forming genes [80]. Carlisle et al. demonstrated that Si promotes bone growth, increases the amount of articular cartilage, and increases the bone mineral content as well as the aminocaproic acid and collagen contents [81]. Jugdaohsingh et al. demonstrated that Si deficiency leads to malformations in bone development and low collagen production [82]. Carlisle et al. reported that Si ions play a key role in the mineralisation of new bone [83]. Hang Liang et al. reported that gold nanoparticle-loaded mesoporous silica and mesoporous silica have immunomodulatory capabilities and can generate a favourable immune microenvironment by stimulating anti-inflammatory responses and promoting the secretion of osteoclastogenic factors by macrophages [84]. In addition, Day et al. reported that Si ions released from the bioactive glass 45S5 can promote the secretion of the vascular growth factors VEGF and bFGF [85]. Similarly, Li et al. reported that Si ions can increase VEGF secretion in fibroblasts and endothelial cells, which in turn upregulates the expression of nitric oxide synthase and effectively stimulates bone angiogenesis [86]. In addition, higher concentrations of calcium and phosphorus are generally favourable for promoting the osteogenic differentiation of BMSCs [87]. However, different calcium−phosphorus ratios also affect cell proliferation and osteogenic differentiation. For example, Pan Jin et al. reported that a higher calcium-to-phosphorus ratio precipitated by bioceramics promoted the proliferation and osteogenic differentiation of BMSCs [87]. Margaret K. Boushell et al. reported that a higher calcium-to-phosphorus ratio promotes chondrocyte mineralisation [88]. Similarly, Rustko Masuyama et al. reported that when fed diets with higher calcium-to-phosphorus ratios, the bone mineral content (BMC) and BMD of the femurs of mice are significantly greater, the osteoid maturation time is significantly reduced, and the bone formation rate is increased [89]. Under the combined effect of various ions, the proliferation and osteogenic differentiation abilities of MSCs were significantly enhanced after treatment with mBG ion products. Furthermore, the production of secreted exosomes was significantly enhanced, and their ability to promote the proliferation and osteogenic differentiation of OBs, as well as bone and vascular regeneration in vivo, increased. Additionally, the immunomodulatory abilities of the exosomes were also significantly enhanced, which is consistent with what has been reported in the literature [19,22,33,84].

Osteoimmunomodulatory therapies based on extracellular vesicles and biomimetic surface strategies from Jiaxiang Bai and Gaoran Ge et al. have shown considerable efficacy in promoting osseointegration studies in bone implants [66,90]. These findings provide ideas for further clinical applications of exosomes with improved bone regeneration, immunomodulation and angiogenic properties. However, future studies are still needed to validate the safety of these exosomes for humans, and additional studies are needed in other large-animal models, such as rabbits, beagle dogs, and pigs, to strengthen preclinical studies.

5. Conclusion

Increasing the production of exosomes by cells and enhancing the pro-bone healing functions of exosomes are the keys to accelerate the application of exosomes in the repair of clinical bone defects. In this study, we prepared mBG and its ionic products and used them to treat MSCs, after which the exosomes produced by the MSCs were collected. The results showed that compared to other groups, Exo-mBG significantly promoted the proliferation, osteogenic differentiation and mineralisation of OBs in vitro. Meanwhile, the Exo-mBGs group significantly promoted the expression of the macrophage M2-type genes, and downregulated the expression of the M1-type genes, compared with the other two groups. In vivo, the Exo-mBG group significantly promoted the healing and angiogenesis of bone tissue at the cranial defects in rats, as well as promoted the M2 polarisation and inhibited the M1 polarisation of macrophages. These effects may be due to the combined higher silicon concentration and higher calcium-to-phosphorus ratio in the mBG ionic products. The present work provides a new scientific basis and technical approach for the repair of bone defects by MSCs-derived exosomes, which supports the application of exosomes in replacement cell therapy.

Funding

This research was supported by the National Natural Science Foundation of China (32000964, 82160577), the Guangdong Province Science and Technology Plan Project (2024A1515012265, 2020B1111560001 and 2022A1515140193), the Key Program for Science and Technology Project of Guizhou Province (ZK [2021] 007), the Program for Science and Technology Project of Guizhou Province. Qiankehe Platform Talents ([2021] 5613), the Hainan Academician Innovation Center (Nanfan Medical Materials and Health Technology Innovation Center) (2022GDASZH-2022020402-01), the Project of Science and Technology Development of Guangdong Academy of Sciences (2022GDASZH-2022010110 and 2020GDASZH-2022030604-01), the Guangzhou Science and Technology Plan Project (202102020362).

Data availability

If possible and applicable, we have deposited data that support the findings of our research in a public repository.

Ethics statement

All animal experiments were performed under the protocol approved by the Institutional Animal Care and Use Committee of Guangdong Quality Supervision and Testing Station for Medical and Health Care Appliances.

Declaration of competing interest

We declare that we have no financial and personal relationships with other people or organizations that can inappropriately influence our work, there is no professional or other personal interest of any nature or kind in any product, service and/or company that could be construed as influencing the position presented in, or the review of, the manuscript entitled.

Acknowledgements

This research was supported by the National Natural Science Foundation of China (32000964, 82160577), the Guangdong Province Science and Technology Plan Project (2024A1515012265, 2020B1111560001 and 2022A1515140193), the Key program for Science and Technology Project of Guizhou Province (ZK [2021] 007), the Program for Science and Technology Project of Guizhou Province. Qiankehe Platform Talents ([2021] 5613), the Hainan Academician Innovation Center (Nanfan Medical Materials and Health Technology Innovation Center) (2022GDASZH-2022020402-01), and the Project of Science and Technology Development of Guangdong Academy of Sciences (2022GDASZH-2022010110, and 2020GDASZH-2022030604-01).

Appendix A. Supplementary data

Supplementary data to this article can be found online at https://doi.org/10.1016/j.jot.2024.09.009.

References

[1] Mckee MD. Management of segmental bony defects: the role of osteoconductive orthobiologics. J Am Acad Orthop Surg 2006;14(10 Spec No):S163–7.
[2] Miron RJ, Gruber R, Hedbom E, Dds PhD NS, Dds YZ, Dds AS, et al. Impact of bone harvesting techniques on cell viability and the release of growth factors of autografts. Clin Implant Dent Relat Res 2013;15(4):481–9.
[3] Oreffo R, Triffitt J. Future potentials for using osteogenic stem cells and biomaterials in orthopedics. Bone 1999;25:5S–9S.
[4] Naohiro Shibuya, Daniel C. Jupiter, Bone graft substitute: allograft and xenograft. Clin Podiatr Med Surg 2015;32(1):21–34.
[5] Koob S, Torio-Padron N, Stark GBR, Hannig C, Stankovic Z, Finkenzeller G. Bone formation and neovascularization mediated by mesenchymal stem cells and endothelial cells in critical-sized calvarial defects. Tissue Eng Part A 2011;17(3):311–21.
[6] Ding DC, Shyu WC, Lin SZ. Mesenchymal stem cells. Cell Transplant 2011;20(1):5–14.
[7] Gauthaman K, Bongso A, Fong CY. Taking stem cells to the clinic: major challenges. J Cell Biochem 2008;105(6):1352–60.
[8] Sweta Rani, Aideen Ryan, Matthew Griffin, Thomas Ritter. Mesenchymal stem cell-derived extracellular vesicles: toward cell-free therapeutic applications. Mol Ther 2015;23(5):812–23.
[9] Cabral J, Ryan AE, Griffin MD, Ritter T. Extracellular vesicles as modulators of wound healing. Adv Drug Deliv Rev 2018;129:394–406.
[10] Golchin A, Hosseinzadeh S, Ardeshirylajimi A. The exosomes released from different cell types and their effects in wound healing. J Cell Biochem 2018;119(7):5043–52.
[11] Mittelbrunn M, Sánchez-Madrid F. Intercellular communication: diverse structures for exchange of genetic information. Nat Rev Mol Cell Biol 2012;13(5):328–35.
[12] Lu J, Wang Q, Sheng J. Exosomes in the repair of bone defects: next-generation therapeutic tools for the treatment of nonunion. BioMed Res Int 2019;2019:1983131.
[13] Watson D, Yung B, Bergamaschi C, Chowdhury B, Bear J, Stellas D, et al. Scalable, cGMP-compatible purification of extracellular vesicles carrying bioactive human heterodimeric IL-15/lactadherin complexes. J Extracell Vesicles 2018;7(1):1442088.
[14] Patel DB, Luthers CR, Lerman MJ, Fisher JP, Jay SM. Enhanced extracellular vesicle production and ethanol-mediated vascularization bioactivity via a 3D-printed scaffold-perfusion bioreactor system. Acta Biomater 2019;95:236–44.
[15] Tauro B, Greening D, Mathias R, Ji H, Mathivanan S, Scott A, et al. Comparison of ultracentrifugation, density gradient separation, and immunoaffinity capture methods for isolating human colon cancer cell line LIM1863-derived exosomes. Methods (San Diego, Calif.) 2012;56(2):293–304.
[16] Nordin J, Lee Y, Vader P, Mäger I, Johansson H, Heusermann W, et al. Ultrafiltration with size-exclusion liquid chromatography for high yield isolation of extracellular vesicles preserving intact biophysical and functional properties. Nanomed Nanotechnol Biol Med 2015;11(4):879–83.
[17] King H, Michael M, Gleadle J. Hypoxic enhancement of exosome release by breast cancer cells. BMC Cancer 2012;12:421.
[18] de Abreu R, Fernandes H, da Costa Martins P, Sahoo S, Emanueli C, Ferreira L. Native and bioengineered extracellular vesicles for cardiovascular therapeutics. Nat Rev Cardiol 2020;17(11):685–97.
[19] Ruan X, Ju C, Shen Y, Liu Y, Kim I, Yu H, et al. Suxiao Jiuxin pill promotes exosome secretion from mouse cardiac mesenchymal stem cells in vitro. Acta Pharmacol Sin 2018;39(4):569–78.
[20] Shyong Y, Chang K, Lin F. Calcium phosphate particles stimulate exosome secretion from phagocytes for the enhancement of drug delivery. Colloids and surfaces. B, Biointerfaces 2018;171:391–7.
[21] Magyari K, Baia L, Vulpoi A, Simon S, Popescu O, Simon V. Bioactivity evolution of the surface functionalized bioactive glasses. Journal of biomedical materials research. Part B, Applied biomaterials 2015;103(2):261–72.
[22] Tsigkou O, Labbaf S, Stevens MM, Porter AE, Jones JR. Monodispersed bioactive glass submicron particles and their effect on bone marrow and adipose tissue-derived stem cells. Adv. Healthc. Mater. 2014;3(1):115–25.
[23] Xynos ID, Edgar AJ, Buttery LDK, Hench LL, Polak JM. Ionic products of bioactive glass dissolution increase proliferation of human osteoblasts and induce insulin-like growth factor II mRNA expression and protein synthesis. Biochem Biophys Res Commun 2000;276(2):461–5.
[24] Z.W.A. B, D.H.A. B, H.L.A. B. Bioglass enhances the production of exosomes and improves their capability of promoting vascularization. Bioact Mater 2021;6(3):823–35.
[25] Newman H, Shih YV, Varghese SJB. Resolution of inflammation in bone regeneration: from understandings to therapeutic applications. Biomaterials 2021;277:121114.
[26] Navegantes KC, Rafaelli DSG, Pereira PAT, Czaikoski PG, Azevedo CHM, Monteiro MC. Immune modulation of some autoimmune diseases: the critical role of macrophages and neutrophils in the innate and adaptive immunity. J.J.o.T.M 2017;15(1):36.
[27] He F, Lu T, Fang X, Tian Y, Li Y, Zuo F, et al. Modification of honeycomb bioceramic scaffolds for bone regeneration under the condition of excessive bone resorption. J.J.o.B.M.R.P.A 2019;107(6):1314–23.
[28] Liu C, Cui Y, Luan J, Zhou X, Han J. Fibroblast growth factor-2 inhibits mineralization of osteoblast-like Saos-2 cells by inhibiting the functioning of matrix vesicles. Drug discoveries & therapeutics 2014;8(1):42–7.
[29] Tian Y, Ma L, Gong M, Su G, Yan X. Protein profiling and sizing of extracellular vesicles from colorectal cancer patients via flow cytometry. ACS Nano 2018;12(1):671–80.
[30] The United States Pharmacopeia 1820-1970. J Am J Hosp Pharm 1970;27(3).
[31] ElBadry KM, Moustafa FA, Azooz MA, El Batal FH, Physics A. Infrared absorption spectroscopy of some bio-glasses before and after immersion in various solutions. IJPAP 2000;38(11):741–67.
[32] Martínez A, Izquierdo-Barba I, Vallet-Regl M. Bioactivity of a CaOSiO 2 binary glasses system. Chem Mater 2000;12(10):3080–8.
[33] Yan-Jye S, Kuo-Chi C, Feng-Huei L. Calcium phosphate particles stimulate exosome secretion from phagocytes for the enhancement of drug delivery. Colloids and surfaces B: Biointerfaces 2018;171:391–7.
[34] Xia W, Chang J. Well-ordered mesoporous bioactive glasses (MBG): a promising bioactive drug delivery system. J Contr Release 2006;110(3):522–30.
[35] Zhu YF, Kaskel S. Comparison of the *in vitro* bioactivity and drug release property of mesoporous bioactive glasses (MBGs) and bioactive glasses (BGs) scaffolds. Microporous Mesoporous Mat 2009;118(1–3):176–82.
[36] Hu Q, Chen X, Zhao N, Li Y, Mao C. Fabrication and characterization of dodecylamine derived monodispersed mesoporous bioactive glass sub-micron spheres. J Sol Gel Sci Technol 2014;69(1):9–16.
[37] Xia Li, Lingxia Zhang, Xiaoping Dong, Jian. Preparation of mesoporous calcium doped silica spheres with narrow size dispersion and their drug loading and degradation behavior. Microporous Mesoporous Mater 2007;102(1–3):151–8.
[38] Lin S, Ionescu C, Pike KJ, Smith ME, Jones JR. Nanostructure evolution and calcium distribution in sol-gel derived bioactive glass. J Mater Chem 2009;19(9):1276–82.
[39] Xynos ID, Edgar AJ, Buttery LDK, Hench LL, Polak JM. Ionic products of bioactive glass dissolution increase proliferation of human osteoblasts and induce insulin-like growth factor II mRNA expression and protein synthesis. Biochem Biophys Res Commun 2000;276(2):461–5.
[40] Hesaraki S, Gholami M, Vazehrad S, Shahrabi SJMS, C E. The effect of Sr concentration on bioactivity and biocompatibility of sol–gel derived glasses based on CaO–SrO. SiO 2–P 2O 5 quaternary system 2010;30(3):383–90.
[41] Colombo M, Raposo G, Théry C. Biogenesis, secretion, and intercellular interactions of exosomes and other extracellular vesicles. Annu Rev Cell Dev Biol 2014;30:255–89.
[42] Kalluri R, LeBleu V. The biology function and biomedical applications of exosomes. Science (New York, NY) 2020;367(6478):640.
[43] Record M, Carayon K, Poirot M, Silvente-Poirot S. Exosomes as new vesicular lipid transporters involved in cell-cell communication and various pathophysiologies. Biochim Biophys Acta 2014;1841(1):108–20.
[44] Wu Z, He D, Li H. Bioglass enhances the production of exosomes and improves their capability of promoting vascularization. Bioact Mater 2021;6(3):823–35.
[45] Henriques-Antunes H, Cardoso R, Zonari A, Correia J, Leal E, Jiménez-Balsa A, et al. The kinetics of small extracellular vesicle delivery impacts skin tissue regeneration. ACS Nano 2019;13(8):8694–707.
[46] Zhang Y, Liu D, Chen X, Li J, Li L, Bian Z, et al. Secreted monocytic miR-150 enhances targeted endothelial cell migration. Molecular cell 2010;39(1):133–44.
[47] Ibrahim A, Marbán E. Exosomes: fundamental biology and roles in cardiovascular physiology. Annu Rev Physiol 2016;78:67–83.
[48] Sansone P, Savini C, Kurelac I, Chang Q, Amato L, Strillacci A, et al. Packaging and transfer of mitochondrial DNA via exosomes regulate escape from dormancy in hormonal therapy-resistant breast cancer. Proceedings of the National Academy of Sciences of the United States of America 2017;114(43):E9066–75.
[49] Kim WS, Kim HK. Tissue engineered vascularized bone formation using in vivo implanted osteoblast-polyglycolic acid scaffold. J. Korean Med. Sci. 2005;20(3):479–82.
[50] Zhu S-J, Choi B-H, Huh J-Y, Jung J-H, Kim B-Y, Lee S-H. A comparative qualitative histological analysis of tissue-engineered bone using bone marrow mesenchymal stem cells, alveolar bone cells, and periosteal cells. Oral Surg Oral Med Oral Pathol Oral Radiol Endod 2006;101(2):164–9.
[51] Kim SW, Her SJ, Park SJ, Kim D, Park KS, Lee HY, et al. Ghrelin stimulates proliferation and differentiation and inhibits apoptosis in osteoblastic MC3T3-E1 cells. Bone 2005;37(3):359–69.
[52] Mizuno M, Kuboki Y. Osteoblast-related gene expression of bone marrow cells during the osteoblastic differentiation induced by type I collagen. Journal of biochemistry 2001;129(1):133–8.
[53] An J, Yang H, Zhang Q, Liu C, Zhao J, Zhang L, et al. Natural products for treatment of osteoporosis: the effects and mechanisms on promoting osteoblast-mediated bone formation. Life Sci 2016;147:46–58.
[54] Merry K, Dodds R, Littlewood A, Gowen M. Expression of osteopontin mRNA by osteoclasts and osteoblasts in modelling adult human bone. J Cell Sci 1993:1013–20.
[55] Stein GS, Lian JB, Owen TA. Relationship of cell-growth to the regulation of tissue-specific gene-expression during osteoblast differentiation. Faseb J 1990;4(13):3111–23.
[56] Li Wenyue, Liu Yunsong, Zhang Ping, Tang Yiman, Zhou M. Interfaces, tissue-engineered bone immobilized with human adipose stem cells-derived exosomes promotes bone regeneration. ACS Appl Materi Interfaces 2018;102(1–3):151–8.

[57] Xin Q, Jieyuan Z, Hong Y, Zhengliang X, Qing L, Xin N, et al. Exosomes secreted by human-induced pluripotent stem cell-derived mesenchymal stem cells repair critical-sized bone defects through enhanced angiogenesis and osteogenesis in osteoporotic rats. Int J Biol Sci 2016;12(7):836–49.
[58] Jieyuan Z, Xiaolin L, Haiyan L, Chunyuan C, Bin H, Xin N, et al. Exosomes/tricalcium phosphate combination scaffolds can enhance bone regeneration by activating the PI3K/Akt signaling pathway. Stem Cell Res Ther 2016;7(1):136.
[59] Xu W, Huang W, Cai X, Dang Z, Hao L, Wang L. Dexamethasone long-term controlled release from injectable dual-network hydrogels with porous microspheres immunomodulation promotes bone regeneration. ACS Appl Mater Interfaces 2024;16(31):40581–601.
[60] Liu X, Yang Y, Li Y, Niu X, Zhao B, Wang Y, et al. Integration of stem cell-derived exosomes with in situ hydrogel glue as a promising tissue patch for articular cartilage regeneration. Nanoscale 2017;9(13):4430–8.
[61] Wu XQ, He WJ, Mu XR, Liu Y, Deng JY, Liu YQ, Nie XQ. Macrophage polarization and diabetic wound healing. Burns Trauma 2022;10:tkac051.
[62] Song Y, Wu H, Gao Y, Li J, Lin K, Liu B, et al. Zinc silicate/nano-hydroxyapatite/collagen scaffolds promote angiogenesis and bone regeneration via the p38 MAPK pathway in activated monocytes. ACS Appl Mater Interfaces 2020;12(14):16058–75.
[63] Lisi L, Ciotti G, Braun D, Kalinin S, Currò D, Dello Russo C, et al. Expression of iNOS, CD163 and ARG-1 taken as M1 and M2 markers of microglial polarization in human glioblastoma and the surrounding normal parenchyma. Neurosci Lett 2017;645:106–12.
[64] Martinez F, Gordon S. The M1 and M2 paradigm of macrophage activation: time for reassessment. F1000prime reports 2014;6:13.
[65] Rőszer T. Understanding the mysterious M2 macrophage through activation markers and effector mechanisms. Mediat Inflamm 2015;2015:816460.
[66] Ge GR, Wang W, Wang Q, Wang M, Wang T, Yu L, et al. Extracellular vesicle clicking on osteoimplants through biomimetic molecular adhesion enables immune-enhanced osseointegration in diabetics. Adv Funct Mater 2024;34(27):18.
[67] Marrella A, Lee T, Lee D, Karuthedom S, Syla D, Chawla A, et al. Engineering vascularized and innervated bone biomaterials for improved skeletal tissue regeneration. Mater Today 2018;21(4):362–76.
[68] Zhang J, Guan J, Niu X, Hu G, Guo S, Li Q, et al. Exosomes released from human induced pluripotent stem cells-derived MSCs facilitate cutaneous wound healing by promoting collagen synthesis and angiogenesis. J Transl Med 2015;13:49.
[69] Qi X, Zhang J, Yuan H, Xu Z, Li Q, Niu X, et al. Exosomes secreted by human-induced pluripotent stem cell-derived mesenchymal stem cells repair critical-sized bone defects through enhanced angiogenesis and osteogenesis in osteoporotic rats. Int J Biol Sci 2016;12(7):836–49.
[70] Liu X, Li Q, Niu X, Hu B, Chen S, Song W, et al. Exosomes secreted from human-induced pluripotent stem cell-derived mesenchymal stem cells prevent osteonecrosis of the femoral head by promoting angiogenesis. Int J Biol Sci 2017;13(2):232–44.
[71] Wu M, Liu H, Zhu Y, Chen F, Chen Z, Guo L, et al. Mild photothermal-stimulation based on injectable and photocurable hydrogels orchestrates immunomodulation and osteogenesis for high-performance bone regeneration. Small 2023;19(28):e2300111.
[72] Hench LL. A genetic theory of bioactive materials. In: Giannini S, Moroni A, editors. Bioceramics. Zurich-Uetikon: Trans Tech Publications Ltd; 2000. p. 575–80.
[73] Bosetti M, Cannas M. The effect of bioactive glasses on bone marrow stromal cells differentiation. Biomaterials 2005;26(18):3873–9.
[74] Li ZM, Chen XF, Lin C, Zhao NR. The in vitro bioactive of sol-gel bioactive glass powders with three-dimensional lamellar structure. Adv Powder Technol 2012;23(1):13–5.
[75] Zhou X, Zhang N, Mankoci S, Sahai N. Silicates in orthopedics and bone tissue engineering materials. Journal of biomedical materials research. Part A 2017;105(7):2090–102.
[76] Beck G, Ha S, Camalier C, Yamaguchi M, Li Y, Lee J, et al. Bioactive silica-based nanoparticles stimulate bone-forming osteoblasts, suppress bone-resorbing osteoclasts, and enhance bone mineral density in vivo. Nanomed Nanotechnol Biol Med 2012;8(6):793–803.
[77] Shie M, Ding S, Chang H. The role of silicon in osteoblast-like cell proliferation and apoptosis. Acta Biomater 2011;7(6):2604–14.
[78] Han P, Wu C, Xiao Y. The effect of silicate ions on proliferation, osteogenic differentiation and cell signalling pathways (WNT and SHH) of bone marrow stromal cells. Biomater Sci 2013;1(4):379–92.
[79] Li Jianyou, Wei Sun. Junying, Effect of ionic products of dicalcium silicate coating on osteoblast differentiation and collagen production via TGF-β1 pathway. J Biomater Appl 2013;27(5):595–604.
[80] Ding SJ, Shie MY, Wang CY. Novel fast-setting calcium silicate bone cements with high bioactivity and enhanced osteogenesis in vitro. J Mater Chem 2009;19(8):1183–90.
[81] Carlisle E. Silicon: an essential element for the chick. Science (New York, NY) 1972;178(4061):619–21.
[82] Jugdaohsingh R, Calomme MR, Robinson K, Nielsen F, Anderson SHC, D'Haese P, et al. Increased longitudinal growth in rats on a silicon-depleted diet. Bone 2008;43(3):596–606.
[83] Carlisle EM. Biochemical and morphological-changes associated with long-bone abnormalities in silicon deficiency. J Nutr 1980;110(5):1046–56.
[84] Hang Liang, Chen Jin, Xiaobo Feng, Xiangyu Deng, Shuilin XJAa. Materials, interfaces, accelerated bone regeneration by gold-nanoparticle-loaded mesoporous silica through stimulating immunomodulation 2019;11(44):41758–69.
[85] Day RM. Bioactive glass stimulates the secretion of angiogenic growth factors and angiogenesis in vitro. Tissue Eng 2005;11(5–6):768–77.
[86] Li HY, Chang J. Bioactive silicate materials stimulate angiogenesis in fibroblast and endothelial cell co-culture system through paracrine effect (vol 9, pg 6981, 2013). Acta Biomater 2019;94. 646-646.
[87] Jin P, Liu L, Cheng L, Chen X, Xi S, Jiang T. Calcium-to-phosphorus releasing ratio affects osteoinductivity and osteoconductivity of calcium phosphate bioceramics in bone tissue engineering. Biomed Eng Online 2023;22(1):12.
[88] Boushell M, Khanarian N, LeGeros R, Lu H. Effect of ceramic calcium-phosphorus ratio on chondrocyte-mediated biosynthesis and mineralization. Journal of biomedical materials research. Part A 2017;105(10):2694–702.
[89] Masuyama Y, Nakaya S, Katsumata Y, Kajita M, Uehara S, Tanaka S, et al. Dietary calcium and phosphorus ratio regulates bone mineralization and turnover in vitamin D receptor knockout mice by affecting intestinal calcium and phosphorus absorption. J Bone Miner. Res 2010;18(7):1217–26.
[90] Bai J, Ge G, Wang Q, Li W, Zheng K, Xu Y, et al. Engineering stem cell recruitment and osteoinduction via bioadhesive molecular mimics to improve osteoporotic bone-implant integration. Research 2022;2022:9823784.